# PHOTOPRODUCTION OF NEUTRAL PIONS FROM HYDROGEN AT FORWARD ANGLES FROM 240 TO 480 MEV

Thesis by

William Scott McDonald

In Partial Fulfillment of the Requirements

For the Degree of

Doctor of Philosophy

California Institute of Technology

Pasadena, California

1957

## ACKNOWLEDGEMENTS

The author wishes to thank Dr. V. Z. Peterson whose suggestions and encouragement during the course of this experiment and the author's graduate residence cannot be sufficiently acknowledged. His work and supervision in the design of the experimental apparatus, the operation of the synchrotron, the taking of the data and subsequent analysis have been indispensable.

The many helpful suggestions of Dr. D. R. Corson of Cornell University, his contributions to the design of the experimental apparatus, his participation in several preliminary experimental runs, and his work in the scanning of the plates are gratefully acknowledged. The suggestion of Dr. R. L. Walker that this experiment would be a useful supplement to his own work in neutral pion photoproduction, as well as his continued interest are appreciated. The interest and encouragement of Dr. R. F. Bacher have been very valuable. The discussions with Dr. G. F. Chew of the University of California concerning his theory have been very instructive. The careful scanning of the plates was largely by Mrs. Hedva Forman and Mrs. Elaine Motta at Cal Tech, and Mrs. Carol Sienko and Mrs. Jane Loeffler at Cornell.

The partial financial support of the U. S. Atomic Energy Commission is gratefully acknowledged.

## ABSTRACT

Recoil protons from the process $\gamma + P \longrightarrow P + \pi^o$ have been detected by nuclear emulsions placed within a hydrogen gas target and used to measure the differential cross section for production of neutral pions. In this manner protons of energies as low as 5 Mev can be detected at laboratory angles corresponding to emission of a pion at center-of-momentum (C. M.) angles as low as $26^o$. This experiment thus supplements that of Oakley and Walker which is in the same range of photon energies (240-480 Mev), but is restricted to pion C. M. angles greater than about $70^o$ due to higher minimum detectable proton energy. Common experimental points provide intercomparison of absolute values. Angular distributions are analyzed in the form $d\sigma/d\Omega = A + B \cos\theta + C \cos^2\theta$ in the C. M. system. The combined Oakley-Walker and present data give the average value of the ratio A/C as $-1.60 \pm 0.10$ in the energy range from 260 to 450 Mev. The coefficient B, which gives the front-back asymmetry, passes through zero below the resonance energy of 320 Mev and is positive at higher energies. The theory of Chew and Low shows that the experimental angular distribution coefficients may be described rather well by magnetic dipole absorption leading to a state of angular momentum and isotopic spin 3/2 together with a small amount of S wave interference.

TABLE OF CONTENTS

# I. INTRODUCTION

The reaction

$$\gamma + P \longrightarrow P + \pi^{o} \qquad (1)$$

was first studied at photon energies above 340 Mev by Walker, Oakley and Tollestrup (1) and by Oakley and Walker (2) at this laboratory*. Each of these experiments measured neutral pion angular distributions in the interval of laboratory photon energies between 260 and 450 Mev. The Walker, Oakley and Tollestrup (1) experiment utilized a proton counter telescope and photon counter to count one $\pi^{o}$ decay photon in coincidence with the recoil proton. The energy and angle of the recoil proton were also measured. Since reaction 1 is a two-body reaction a knowledge of the recoil proton energy and angle and the direction of the incident photon makes it possible to calculate the energy of the incident photon and the angle of the meson in the center-of-momentum (C.M.) system. The coincidence requirement has the advantage of identifying the reaction but it decreases the counting rate. This experimental method also suffers from the fact that the absolute efficiency of the photon counter enters into the cross section. For these reasons the experiment of Oakley and Walker (2) who used a magnetic spectrometer and counter system to measure the energy and angle of the recoil proton only was considered the more accurate of the two experiments.

The results of the above two experiments were in reasonable agreement with each other, but the angular distributions measured

---

*Synchrotron Laboratory, California Institute of Technology.

were restricted to pion C.M. angles between $70^{o}$ and $150^{o}$, with no measurements at more forward angles. The lower limit on pion angles was determined by the lowest energy proton which the counters could detect. Self absorption in the target and counters set this low energy limit at about 25 Mev. Protons of lower energy than this come out at more backward angles in the C.M. system and hence correspond to pions at forward C.M. angles.

The primary purpose of the present experiment is to extend the angular distributions measured by Oakley and Walker (2) to more forward pion C.M. angles. To accomplish this it was necessary to measure the energy and angular distributions of lower energy recoil protons. This was done by placing nuclear emulsions inside a hydrogen gas target. The minimum detectable recoil proton energy (5 Mev) was, therefore, limited only by the range in the target gas. It was thus possible to obtain differential cross section measurements for pion angles as low as $26^{o}$ (C.M.). Measurements were made for laboratory photon energies between 240 and 480 Mev.

If differential cross sections, $d\sigma/d\Omega$, at a given photon energy and various pion C.M. angles, $\theta$, are fitted to a formula of the type

$$d\sigma/d\Omega = A + B \cos\theta + C \cos^{2}\theta \qquad (2)$$

the coefficients A, B and C may be calculated at that energy. This assumes that meson production is in S and P states only. In the present paper the new results are taken together with those of

Oakley and Walker (2) and new A, B and C coefficients are computed in the energy interval between 260 and 450 Mev. The same beam monitor was used in both experiments, and the results of both experiments agree with each other within experimental uncertainty in the region near $\theta = 90^{\circ}$, where they overlap. The value of the A coefficient, which is determined by the cross section at $90^{\circ}$, is changed very slightly. However, the addition of new results of comparable statistical weight at forward angles makes possible a more accurate determination of the B and C coefficients than is possible from data which are restricted to essentially the backward hemisphere only.

## II. THEORY

Photomeson production may be analyzed in terms of general angular momentum arguments without recourse to any specific meson theory. Before such an analysis can be made, however, the pion spin and parity must be known. The spin of the positive pion may be deduced by applying the principle of detailed balance to the reaction

$$P + P \longrightarrow \pi^+ + D \qquad (3)$$

and its inverse. Experimental investigations of these reactions are compared in reference (3) where it is concluded that the positive pion has spin zero. Presumably the negative pion has this same spin. Steinberger, Panofsky and Steller (4, 5) have shown that the neutral pion decays into two gamma rays. From this it can be shown (6) that the spin of the neutral meson cannot be unity but must be zero or even and is most likely zero. Investigation of the absorption of negative pions in deuterium by Panofsky, Aamodt and Hadley (7) together with the theoretical analysis of Brueckner Serber and Watson (8) give evidence that the pion is a pseudoscalar particle. With this information regarding the spin and parity of the pion, Feld (9) has made an analysis of photomeson production on the basis of angular momentum considerations. His results are summarized in the following table. The second column gives the total angular momentum, J, and parity of the state, the fourth column denotes the states by the usual spectroscopic notation, and the last column is the expected dependence of the cross section

| $\gamma$ ray absorbed | Intermediate state | $\ell$ of meson | $\ell_J$ | W(θ) | π momentum dependence |
|---|---|---|---|---|---|
| Mag. dipole | 1/2+ | 1 | $P_{1/2}$ | constant | $q^3$ |
| Mag. dipole | 3/2+ | 1 | $P_{3/2}$ | $5-3\cos^2\theta$ | $q^3$ |
| Elect. dipole | 1/2- | 0 | $S_{1/2}$ | constant | $q$ |
| Elect. dipole | 3/2- | 2 | $D_{3/2}$ | $5-3\cos^2\theta$ | $q^5$ |
| Elect. quad. | 3/2+ | 1 | $P_{3/2}$ | $1+\cos^2\theta$ | $q^3$ |
| Elect. quad. | 5/2+ | 3 | $F_{3/2}$ | $1+6\cos^2\theta -5\cos^4\theta$ | $q^7$ |

near threshold on the momentum, q, of the π meson in the C.M. system. W(θ) is the angular distribution.

The results listed in the table hold only for pure angular momentum and parity states. If there is a mixture of states the result is more complicated due to interference effects. If only S and P states of the meson are considered, Gell-Mann and Watson (10) have shown that the angular distribution is given by

$$\begin{aligned} W(\theta) = {} & |E_1|^2 + |M_1|^2 + \tfrac{1}{2}|M_2|^2 [5 - 3\cos^2\theta] \\ & + \tfrac{1}{8}|E_2|^2 [1 + \cos^2\theta] \\ & - 2\,\mathrm{Re}\,[E_1^* (M_2 - M_1 - \tfrac{1}{2}E_2)]\cos\theta \\ & - \tfrac{1}{2}\,\mathrm{Re}\,[E_2^* (M_2 - M_1)][3\cos^2\theta - 1] \\ & - \mathrm{Re}\,[M_2^* M_1][3\cos^2\theta - 1] \end{aligned} \qquad (4)$$

where $E_1$, $E_2$, $M_1$, $M_2$ are the matrix elements of the elect.

dipole $S_{1/2}$, elect. quad. $P_{3/2}$, mag. dipole $P_{1/2}$ and mag. dipole $P_{3/2}$ states respectively. Note that if there is no electric dipole contribution to the cross section the coefficient of cos θ in equation 4 vanishes. Therefore, if experimental cross sections are analyzed in the form of equation 2, a non-zero value of B implies a finite S wave contribution.

Angular momentum considerations alone do not distinguish between different charge states of the meson and nucleon. If the assumption of charge independence is invoked the isotopic spin, T, is introduced as an additional quantum number. The two reactions

$$\gamma + P \longrightarrow P + \pi^{o} \tag{1}$$

and

$$\gamma + P \longrightarrow N + \pi^{+} \tag{5}$$

differ only in the relative amplitudes of the final state wave function in the isotopic spin 3/2 and 1/2 components. As shown by Feld (9), the reaction amplitudes are

$$A_J(\pi^{o}) = \sqrt{2/3}\ A_{J,\,T=3/2} + \sqrt{1/3}\, A_{J,\,T=1/2} \tag{6}$$

for the first reaction, and

$$A_J(\pi^{+}) = \sqrt{1/3}\ A_{J,\,3/2} - \sqrt{2/3}\ A_{J,\,1/2} \tag{7}$$

for the second.

Strong coupling theory predicted a resonance in pion-nucleon scattering of the $P_{3/2}$ state with isotopic spin 3/2. Experiments (11)

have shown an indication of this resonance. Brueckner and Case (12) then suggested that magnetic dipole transitions to the $J = 3/2$, $T = 3/2$ state might be important in pion photoproduction. The Cal Tech experiments (1, 2) indicated that the neutral pion photoproduction cross section reaches a fairly sharp maximum at a photon energy of 320 Mev and then falls off in a manner suggestive of a resonance. If $\pi^o$ production took place solely by magnetic dipole absorption into the $J = 3/2$, $T = 3/2$ state, the angular distribution would be proportional to $5-3\cos^2\theta$ so that a fit of the experimental data to equation 2 would give $-A/C = 5/3 = 1.67$ and $B = 0$. The Oakley and Walker (2) data gave an average value of $1.22 \pm 0.10$ for the ratio $-A/C$ in the region of the resonance, which indicated that other matrix elements, such as the electric quadrupole to give a $J = 3/2$, $T = 3/2$ state, might also be important. Their experimental uncertainties for B were too large to draw very positive conclusions concerning its value. As shown later the present experiment assigns a value to $-A/C$ more nearly consistent with pure magnetic dipole absorption, but B appears to be non-zero at resonance energy and above.

Watson, Keck, Tollestrup and Walker (13) have made a partial wave analysis of the existing experimental photomeson cross sections based on the phenomenological theory of Gell-Mann and Watson (10). The analysis is made in terms of matrix elements for photoproduction into states of definite angular momentum and isotopic spin. It is assumed that but few states of orbital angular momentum are involved in pion-nucleon interactions and that the $J = 3/2$, $T = 3/2$ state is one of strong, attractive interaction. A

full comparison with experiment can only be made by combining data on charged and neutral pion production. For this reason it is important to obtain cross sections for both positive and neutral pion production whose absolute values may be compared. The neutral pion experimental data adopted by them in their analysis were based on the experimental results of Oakley and Walker (2) at high energies (above 290 Mev) and fit fairly well the results of Goldschmidt-Clermont et al. (14) below this energy. Older $\pi^0$ photoproduction experiments which were not given as much weight were those of Silverman and Stearns (15) and Walker, Oakley and Tollestrup (1).

A non-relativistic theory of the Yukawa type has been developed by Chew and Low (16, 17). The theory achieves comparative simplicity by eliminating antinucleons and nucleon recoil. It has the advantage, in contrast to the phenomenological theories, of introducing very few parameters: mainly the renormalized coupling constant and a pion momentum cut off. The theory has recently been extended by Chew, Low, Nambu and Goldberger (18). A comparison of the present experimental results with this theory will be given in a later section.

## III. EXPERIMENTAL PROCEDURE

The experimental apparatus is shown in Fig. 1. This arrangement is similar in principle to that of Goldschmidt-Clermont, Osborne and Scott (14) who measured neutral pion differential cross sections for gamma ray energies from 170 to 340 Mev with nuclear emulsions.

The 500 Mev bremsstrahlung beam of the California Institute of Technology electron synchrotron passed through a tapered lead collimator and secondary beam "scraper" into the hydrogen tank through a 0.019" stainless steel window and out through a 0.031" stainless steel exit window. It was found necessary to make the target tank quite long in order to keep the entrance window and emulsion chamber well separated from each other and hence to prevent excessive electron background produced in the entrance window from blackening the emulsions. Background electrons produced in the windows were deflected by a 10,000 gauss magnetic field and absorbed in thick lead walls surrounding the entrance tube (see Fig. 1). The total exposure was $3.84 \times 10^{14}$ Mev as measured by the same monitor ionization chamber used by Oakley and Walker (2) (hereafter referred to as O. W.).

The hydrogen was cooled by a dry ice and alcohol mixture held in a styrofoam-insulated compartment enclosing the target. The average hydrogen gas pressure was 367 P.S.I. Due to a leak in the target tank the gas pressure varied from 440 to 240 during the exposure. An accurate time-pressure record was kept during the run and the error in the integrated (density x exposure) value

is estimated to be less than 3%. The variation in gas pressure also produces an uncertainty of about ± 50 microns (emulsion equivalent) in the proton hydrogen range. Fortunately, this does not seriously affect the resolution in range required to define the cross sections.

Nuclear emulsions exposed to hydrogen gas at room temperature for a few minutes will be badly blackened when developed because of reduction of the AgBr. The temperature coefficient of this reaction is such that hydrogen at dry ice temperature produces no blackening after many hours exposure. Cooling the gas, therefore, has the dual purpose of preventing emulsion blackening and increasing the gas density.

The brass emulsion chamber held two pairs of 600 micron C2 pellicles placed on opposite sides of the beam center-line (see Fig. 2). A similar emulsion geometry was used by Panofsky and Fillmore (19). This geometry has the advantage that if the measurement of cross section is based on the sum of the tracks measured in paired plates, any error due to an error in beam centering is reduced. The beam was carefully centered and its diameter (19/32") measured with x-ray film. The distribution in dip angle of tracks found in each pellicle was also in agreement with a well-centered beam.

Pellicles were used instead of glass-backed emulsions because it was found that emulsion bonded to glass cracked when exposed to the cold hydrogen gas. One pellicle at each of the four positions around the beam was sufficient to stop protons in the low

energy range under investigation. This made it possible to avoid the time consuming operation of tracing tracks through a pellicle stack. Since the protons were required to stop in the emulsion, range was used to determine the energy.

As a check on the normalization of this experiment relative to that of O. W. we have measured some cross sections already measured by them. To accomplish this it was necessary to stop protons of a higher energy in the emulsion than could be stopped with a single pellicle. Therefore, protons of higher energy were slowed down by a carbon absorber placed over the rear portion of each pellicle. Protons passing through the front, bevelled edge of the carbon absorber and stopping in the emulsion constitute the high energy or "under carbon" data of the experiment.

After processing, one pair of emulsions was sent to Cornell for scanning and the other was scanned by the Cal Tech emulsion group. The plates were scanned for proton endings and each track was traced back to the point at which it entered the emulsion surface. The scanning was done using 55x oil immersion objectives and 15x flat field eyepieces. The visual appearance of each track was sufficient to distinguish protons from the stopping charged pions in the emulsion. Identifying protons at the end of their range makes the scanning efficiency energy-independent, since all track endings have the same appearance.

The projected range as well as the projected angle and the dip angle of each track at the emulsion surface was measured. The first 100 microns of track was used to measure angles. From

these data the polar angle of emission and initial residual range of the proton were computed. The range is estimated to be accurate to within $\pm 2^{o}/o$, and the measured angles to $\pm 0.3$ degrees. These data also made it possible to project back each track to see if its emulsion trajectory was consistent with the hypothesis that the track came from the direction of the beam. This procedure permitted discrimination against background protons, such as cosmic ray protons, produced by reactions taking place outside of the hydrogen gas. Projecting back each track also gave its range in the hydrogen gas.

Each track was recorded on a kinematic plot, an example of which is shown in Fig. 3. This plot represents $58^{o}/o$ of the total "bare emulsion" data i.e. data not including tracks which passed through the carbon absorber. Each point represents one proton track. The range in gas is included and is expressed in microns of emulsion equivalent. The solid curved lines in Fig. 3 are lines of constant photon energy, k, and of constant cos $\theta$, where $\theta$ is the pion C.M. angle*. The data are thus presented in convenient form for computing cross sections. The center-of-momentum differential cross section, $d\sigma/d\Omega$, for photoproduction of $\pi^{o}$ mesons at an angle $\theta$ by photons of energy k is

$$Y = \frac{d\sigma}{d\Omega} n N(k) \cdot \Delta k \cdot \Delta(\cos\theta) (LWZ/d^{2}) \qquad (8)$$

where Y is the yield of protons from the $\pi^{o}$ reaction in the photon

---

*The kinematics of reaction 1 were computed on an I.B.M. Type 604 Electronic Calculating Machine.

energy interval $\Delta k$ and cos $\theta$ interval $\Delta(\cos\theta)$. N(k) is the number of photons per unit photon energy interval at the photon energy k, and n is the number of hydrogen atoms per $cm^3$. L is the length (parallel to the beam) of the area scanned, which is also the effective target length. W is the width of the area scanned. Z is the offset distance from the beam center to the plate and d is the perpendicular distance from the beam center-line to the center of the scan area (see Fig. 2). Measuring Z and d from the beam center rather than integrating over the finite beam diameter introduces an uncertainty of no more than 1% in the effective solid angle.

It was necessary to take the finite beam size into account, however, in order to obtain cross sections in the high-proton-energy region of the "bare emulsion" data. This is because the maximum range a proton may have in the emulsion, depends upon the dip angle at which it enters the emulsion surface, and hence on the distance from the beam center-line of the proton's point of origin. The dashed horizontal lines in the upper part of Fig. 3 show this effect, the upper and lower lines corresponding to protons having the minimum and maximum possible dip angles respectively. Kinematic intervals were chosen in computing cross sections so that the correction necessary for this "finite beam effect" did not exceed 6%. Four of the cross sections listed in Table I were so corrected.

In the case of the "under carbon" data, cross sections cannot be calculated directly from equation 8 without first correcting for the effect of the carbon absorber. This correction is introduced

because of the fact that there is only a narrow interval of azimuthal angles, $\delta\phi$, (see Fig. 4) into which protons at a given energy and polar angle can be emitted and come to rest in the emulsion. Protons of that energy and polar angle emitted outside the azimuthal interval $\delta\phi$ will not end in the emulsion and hence not be recorded; they either stop in the carbon before entering the emulsion or pass all the way through the emulsion without stopping. The under carbon region of the plate was scanned for proton endings until all tracks entering the emulsion surface between $\bar{y} = \bar{y}_1$ and $\bar{y} = y_2$ were found, where $\bar{y}$ is the perpendicular distance back from the front edge of the carbon of the emulsion-entrance point. If the width of the scan area corresponds to an azimuthal angular interval, $\Delta\phi$, then the fraction of protons of a given energy and polar angle of emission that fall within the interval where they are detected is

$$\varepsilon = \delta\phi/\Delta\phi \tag{9}$$

where azimuthal symmetry has been assumed. Fig. 5 is a plot of $\varepsilon$ vs. R sin $\theta_p$ where the limits of $\bar{y}$ are $\bar{y}_1 = 5$ mm, $\bar{y}_2 = 10$ mm, R is the total range in microns of emulsion equivalent and $\theta_p$ is the polar angle of the proton. Cross sections may now be computed from equation 8 provided that the number of tracks found at a given R and $\theta_p$ is corrected by dividing by the appropriate value of the geometrical detection efficiency, $\varepsilon$. Kinematic limits on k and cos $\theta$ were chosen so that the average value of $\varepsilon$ for the "under carbon" data was 0.6.

The total range, R, of the "under carbon" tracks was

calculated as follows,

$$R = R_h + R_c + R_e \tag{10}$$

where $R_h$, $R_c$ and $R_e$ are the ranges in hydrogen, carbon and emulsion respectively, all expressed in microns of emulsion equivalent*. If it is assumed that all tracks originate at the beam center-line, the range in hydrogen is given by

$$R_h = a/\sin \theta_P \tag{11}$$

where "a" is a parameter depending on the relative stopping powers of hydrogen and emulsion. All "under carbon" tracks passed through the front, bevelled edge of the carbon block, and the bevel angle of $12^o$ was so chosen that the plane containing the track and a line parallel to the beam center-line would be essentially normal to the absorber. Under these conditions $R_c$ is given by

$$R_c = by/\sin \theta_P \tag{12}$$

where "b" is a parameter depending on the relative stopping powers of the carbon and emulsion and has an average value of 0.606 if y is in microns.

The effect of the finite beam size has been taken into account in the calculation of the "under carbon" detection efficiency by dividing the beam into four equal parts and calculating the efficiency for each part. In doing this a constant intensity over the area of the beam was assumed. The average value of the efficiency obtained in this calculation was within $1^o/o$ of that obtained if it is assumed that all protons originate on the beam center-line.

---

*In this experiment all emulsion ranges were related to proton energy using the range-energy relation of Fay, Gottstein and Hain (20). Hydrogen and carbon ranges were taken from the range-energy relations of Aron, Hoffman and Williams (21).

## IV. BACKGROUND

For protons produced in reaction 1 by 500 Mev bremsstrahlung, the maximum laboratory angle of emission is about 71°. Fig. 3 shows protons at angles greater than this. A few of these events may be accounted for as $\pi^o$ protons scattered by the hydrogen and emulsion into the angular region beyond the kinematic cutoff. The bulk of these events, however, is due to reactions other than the $\pi^o$ reaction, and it is necessary to correct the $\pi^o$ cross sections by taking these reactions into account. There are a number of possible sources of background, which are discussed below.

### A. Protons from sources outside the gas

Although x-ray pictures taken of the collimated beam show ample clearance between the beam and the collimators, we have sought further evidence of background from the lead or brass surrounding the chamber. If a portion of the beam struck one side of the shielding the background yield would be expected to vary from plate to plate. However, the background per unit solid angle is the same well within statistics for each of the four plates. Hence, we consider this source of background unlikely. A uniformly-irradiated-shielding source of background also seems unlikely. The trajectory of each track was traced back to see if it came from the target region where the beam was striking the gas. About 12% of all protons entering the emulsion surface appeared to come from areas other than the bombarded gas. These can all be accounted for as cosmic ray tracks present in the emulsion and are qualitatively similar to the tracks found in an unexposed control plate of

the same emulsion batch.

B. Protons from pion pair production

The maximum laboratory angle that a proton from the reactions

$$\gamma + p \longrightarrow p + \pi^+ + \pi^- \qquad (13)$$

$$\gamma + p \longrightarrow p + \pi^o + \pi^o \qquad (14)$$

can come out at is 47 degrees, where the photon energy is 500 Mev. This angle is outside the angular interval from which the cross section data were taken.

C. The Compton Effect

Compton recoil protons may be produced in the angular interval from 0 to $90^o$. Recent experimental results (22) show that the Compton proton cross section may be as high as 15 times the Thomson cross section. Such a cross section would produce a proton contribution amounting to less than $3^o/o$ of the total protons observed.

In order to be detected in the present experiment a proton must have an energy of at least 5 Mev, corresponding to an angle of $81^o$ for a Compton proton produced by a 500 Mev gamma ray. Compton protons may therefore be present in the angular region between $71^o$ and $81^o$ beyond the $\pi^o$ proton kinematic angular limit. The background in this angular region is slightly larger than that at angles beyond $81^o$ but this effect can be completely accounted for by the scattering of $\pi^o$ protons into the $71^o$ and $81^o$ interval. Detection of the Compton effect is therefore beyond the resolution

of the present experiment because it is masked at angles beyond the $\pi^o$ kinematic limit by scattered $\pi^o$ protons and the background which in the next section is shown to be due to impurities in the gas.

D. Protons from impurities in the gas

The histogram in Fig. 6 shows the angular distribution of background protons with energy less than 20 Mev at angles between $80^o$ and $105^o$. The latter angle is the minimum geometrical cutoff angle defined by the shielding. Protons from the $\pi^o$ reaction have little chance of being scattered into this angular region, so that the protons in this region must come from other processes. As shown in Fig. 6 the angular distribution is consistent with isotropy. The energy spectrum of these background protons is measured to obey an $E^{-1.6\pm0.3}$ law where E is the proton energy. Levinthal and Silverman (23) have measured the angular distribution and energy spectrum for protons from 7 to 70 Mev produced by 320 Mev bremsstrahlung on carbon. They found an isotropic angular distribution for 10 Mev protons and an energy spectrum of the form $E^{-S}$ where $S = 1.7\pm0.1$ for carbon and varies slowly with atomic number. Absolute photoproton production cross sections for nuclei exposed to 300 Mev bremsstrahlung were measured by Keck (24). Study of photostars produced by 500 Mev bremsstrahlung (25) indicates that Keck's cross sections may be extrapolated to 500 Mev by multiplying them by a factor of 2.5.

Using these results, the observed background angular distribution, energy spectrum, and magnitude can all be accounted for by a nitrogen impurity of 0.17 mole per cent in the hydrogen

gas of the target. An analysis of the actual gas used in the target was not made, but this impurity figure is consistent with the values found by mass spectrographic analyses of hydrogen from the same tank used both prior to, and after, the experimental run. The background protons were therefore attributed to reactions with the nuclei of the impurities, mostly nitrogen, as was found to be the case in the similar emulsion experiment of Goldschmidt-Clermont, Osborne and Scott (14). The $\pi^o$ cross sections were corrected by subtracting the background contribution assuming an isotropic angular distribution and an $E^{-1.7}$ energy spectrum. In the energy interval in which the bulk of the background is found the assumption of angular isotropy is an excellent one. At higher energies, approaching 40 Mev, where the photoproton angular distribution begins to show a forward peaking, the background becomes negligible because of the rapid fall off with proton energy. The background correction varies between 5°/o and 32°/o and averages 15°/o.

## V. CORRECTIONS AND UNCERTAINTIES

The uncertainties in the experiment may be divided into three types: those affecting only the absolute cross section, those affecting the relative cross sections, and random statistical uncertainties.

### A. Uncertainties which affect the absolute cross section

#### 1. Absolute beam monitor calibration

This is estimated to be 7%, as discussed in reference (2), and is not included in the uncertainties assigned to the cross sections in Table I.

#### 2. Average target gas density

This is estimated at 3% and is included in the assigned uncertainties.

#### 3. Scanning efficiency

The scanning efficiency was measured by duplicate scanning to be $95 \pm 2\%$ on three of the plates contributing a total of 1288 events used in the cross section calculations (see Table II). On the fourth plate the scanning efficiency was $75 \pm 3\%$, the reduced efficiency being attributed to a darkening of the emulsion during processing. A total of 237 events were used from this last plate giving a grand total of 1525 events from all four plates. The cross sections have been corrected for these efficiencies and the scanning efficiency uncertainty is included in the uncertainty assigned to the cross sections.

4. Geometrical uncertainties

Uncertainties due to beam centering (19) and measuring of geometrical distance have been estimated as less than 2°/o and are included in the assigned uncertainty. A $1\frac{1}{2}$°/o correction for the measured solid angles was made to take account of emulsion contraction due to exposure at a temperature less than that at which the emulsions were scanned.

B. Uncertainties which affect the relative cross sections

1. Background

The background correction varies from 5°/o to 32°/o with an average value of 15°/o. This correction is based on 190 events and believed accurate within 15°/o. Therefore, the background introduces an uncertainty which varies from less than 1°/o to about 5°/o. This uncertainty is included in the uncertainty assigned to the cross sections.

2. Uncertainty in proton range and angle

The emulsion range measurements are estimated to be accurate within $\pm$ 2°/o. The variation in hydrogen gas pressure introduces an additional uncertainty of $\pm$ 50 microns of emulsion equivalent. The uncertainty in reading the proton angle is about 0.3°. This is smaller than the angular uncertainty due to scattering in the gas and emulsion which is estimated to have an R.M.S. spread varying from $\pm$ 3° to $\pm$ 1° for protons of 400 to 2000 microns total range (emulsion equivalent). If all proton ranges and angles were actually in error by an amount equal to the value of the estimated uncertainties, then the error introduced in the pion C.M.

angles for the cross sections listed in Table I would be about $1^{o}$ and the error in photon energy would vary from 10 to 30 Mev with an average of 20 Mev. The density of events in Fig. 3 varies slowly enough so that scattering introduces negligible correction to the cross section except near the kinematic limit, where the density varies abruptly. The 450 Mev point is the only point requiring a correction, which is calculated to be $12 \pm 6\%$, the assigned uncertainty being due to the uncertainty in the R.M.S. scattering angle of the proton.

C. Random statistical uncertainties

These are the counting statistics and are shown for the present experimental points as the inner uncertainties in Figs. 7, 8 and 9. The statistical uncertainties shown are standard deviations.

Since our data are most useful when combined in an angular distribution with the data of O. W., we have shown those uncertainties which affect our data relative to theirs. This includes all but the beam-monitor-calibration uncertainty, and is typically $10\%$.

## VI. DIFFERENTIAL CROSS SECTIONS COMPARED WITH OTHER DATA

The differential cross sections for the "bare emulsion" data are given in Table I. These cross sections are based on the data tabulated for each of the four plates in Table II. In Table III are summarized the "under carbon" cross sections selected to overlap previous measurements of O. W. The weighted average of the ratio of the cross sections of Table III to the corresponding ones of O. W. is $1.02 \pm 0.09$. Because of this agreement between the two experiments we have not normalized the absolute values obtained in this experiment.

Differential cross sections for mean photon energies of 260, 300, 320, 360, 400 and 450 Mev are shown in Figs. 7, 8 and 9. The solid points are the measurements of O. W. and the open points are the present measurements. Actually O. W. made measurements at 270 and 295 Mev. The excitation functions given by them have been used to calculate cross sections at 260 and 300 Mev in order to compare directly with the present work. The solid curves of Figs. 7, 8 and 9 are least squares fits to the observed data from both experiments, assuming an angular distribution in the form of equation 2. The dashed curves of Figs. 8 and 9 are drawn from the A, B, C coefficients given by O. W. *, based on their data only. It is clear that the new measurements have made significant changes

---

*These A, B, C coefficients are taken from the solid curve of Fig. 9 of reference (2). The requirement that the cross section remain positive at all angles has influenced their choice of B and C at 320 Mev to values more positive than that indicated by their data alone. With the new coefficients, obtained by least squares fit, no difficulty with negative cross sections is encountered.

in the angular distribution coefficients. These changes are particularly evident at energies near resonance where the cross sections at forward angles predicted by the O. W. angular distribution coefficients fall well below the measured values. This reflects the fact that accurate determination of the B and C coefficients requires data at both forward and backward angles.

Goldschmidt-Clermont et al. (14) have measured $\pi^o$ cross sections at M.I.T. for gamma ray energies from 170 Mev to 340 Mev. The absolute normalization of the results quoted by them is based on the adjustment of their monitor calibration to agree with monitor calibrations of the Cornell Synchrotron and Illinois Betatron Laboratories which are in mutual agreement. The beam monitor calibration at the Cal Tech Synchrotron Laboratory is such that on this basis alone the absolute cross sections measured by O. W. and the present experiment would be 5 per cent lower than those measured at Cornell and Illinois (26) (and therefore M.I.T.). Above 280 Mev the cross sections given by Goldschmidt-Clermont et al. are considerably lower than the O. W. results, a fact which is perhaps due to the difficulties in obtaining data so near the upper end of the M.I.T. bremsstrahlung spectrum. The M.I.T. results in the energy interval $k \approx 240$-$280$ Mev are included in Fig. 7, along with the present data and the O. W. data. The agreement seems reasonably good.

## VII. ANGULAR DISTRIBUTION COEFFICIENTS

The final A, B and C coefficients are listed in Table IV and plotted in Fig. 10 as a function of photon energy. The solid curves for A, B and C are a visual fit to the present results and at low energies are drawn to fit the recent Illinois results of Koester and Mills (27).

The dashed curves for A and C in Fig. 10 are the experimental values of $A^{o}$ and $C^{o}$ adopted in the partial wave analysis of the photomeson cross sections by Watson, Keck, Tollestrup and Walker (13). The dashed curve for B is that given by O. W. and is based on their data and the M.I.T. (14) data. Since the value of B depends on the front-to-back ratio the error for this coefficient is rather large in the O. W. experiment.

Above 260 Mev it is clear that the present results have not changed A appreciably, but that C has become considerably less negative. The ratio A/C from 260 to 450 Mev is changed to an average value $-1.60 \pm 0.10$ as contrasted to the value $-1.22 \pm 0.10$ obtained by O. W. If neutral pions were produced only by magnetic dipole absorption leading to a state of angular momentum $J = 3/2$, then the ratio of A/C would be $-5/3 = -1.67$ which is consistent with the new experimental value.

A pure magnetic dipole interaction would imply $B = 0$. However, the solid curve for B in Fig. 10 shows that B becomes positive somewhat below resonance and is definitely positive at energies above resonance. The non-zero value for the interference term, B, above resonance, indicates a finite amount of S wave production in this energy region.

Arguments for the existence of S-wave production (i.e., non-zero values of B) at low energies have been given by Koester and Mills (27), in analyzing their total cross section and 135° differential cross section measurements. The assumption that $B \approx 0$ leads them to deduce values of A/C in violent disagreement with the theory of Chew and Low (16, 17), whereas the magnetic dipole value of $A/C \approx -5/3$ requires B to become so negative as to give negative 0° cross sections. They conclude that finite negative values of B are required below about 210 Mev. In Fig. 10 we have plotted the Illinois values of A, B, and C obtained by assuming the zero degree cross section is actually zero ($A + B + C \approx 0$). When calculated in this manner the coefficient C becomes positive at about 190 Mev (see Fig. 10) and the curves for B and C cross each other near 205 Mev. The magnitudes of A and C are substantially smaller than those based on the M.I.T. (14) data.

The uncertainties assigned to the A, B and C coefficients above 260 Mev are based on the uncertainties assigned to the O. W. and present differential cross sections. If the ratio of the present results to those of O. W. were in error by 9% due to an error in our absolute scale (see Table III), the values of the B and C coefficients would change by about the uncertainty shown in Fig. 10.

## VIII. TOTAL CROSS SECTIONS

Total cross sections are shown in Fig. 11. The solid curve below 245 Mev are the total cross sections measured by Koester and Mills (27). The solid curve above 245 Mev and the dashed curve are obtained from the respective A and C curves in Fig. 10 by means of the formula

$$\sigma_T = 4\pi (A + C/3) \tag{15}$$

where $\sigma_T$ is the total cross section and the formula is obtained by the integration of equation 2.

## IX. COMPARISON WITH THE THEORY OF CHEW AND LOW

A comparison of the present experimental results with the predictions of the theory of Chew and Low (see page 8) will now be made. This theory has already had some success (27) in describing neutral photoproduction at energies below resonance. A recent relativistic extension (18) of this theory has clarified some points in the older cut-off model (16, 17). Chiefly there has been a clarification of the kinematics. In particular, the question of when to use $\nu$ (the photon C.M. momentum) and when to use w (the total pion C.M. energy), which in the limit of the static nucleon assumed in the cut-off model were equal, has been resolved. Also in the older theory there was some question of when to use the phase space factor $(1 + w/M)^{-1}$, where M is the nucleon mass. The newer results show that this factor appears in the positive meson photoproduction cross section but not in the cross section for neutral production.

Let the complete neutral photoproduction amplitude be denoted by $F_{\pi^o, p}$. The differential cross section for meson production in the C.M. system is

$$d\sigma/d\Omega = q/\nu \quad |F_{\pi^o, p}|^2 \tag{16}$$

where q is the meson C.M. momentum. The amplitude is split as follows

$$F_{\pi^o, p} = F^{(+)} + F^{(0)} \tag{17}$$

If negative and positive photomeson-production are also considered,

their respective amplitudes are given by

$$F_{\pi^+,N} = \sqrt{2}\,(F^{(-)} + F^{(0)}) \tag{18}$$

$$F_{\pi^-,P} = -\sqrt{2}\,(F^{(-)} - F^{(0)}) \tag{19}$$

Since we restrict ourselves to neutral production we need only define $F^{(+)}$ and $F^{(0)}$. The main contribution to the cross section is produced by $F^{(+)}$, where

$$\begin{aligned}\frac{1}{ef}\,F^{(+)} &= \bar{q}\cdot(\bar{\nu}\times\bar{\varepsilon})\,\frac{(g_p-g_n)}{4Mf^2}\,h^{(++)} \\ &+ i\,\bar{\sigma}\cdot\bar{q}\times(\bar{\nu}\times\bar{\varepsilon})\,\frac{(g_p-g_n)}{4Mf^2}\,h^{(+-)} \\ &- \bar{\sigma}\cdot\bar{\varepsilon}\,\frac{2}{3}(\delta_1-\delta_3)\,F_S\end{aligned} \tag{20}$$

In this equation $\bar{\sigma}$ is the nucleon spin vector and $\bar{\varepsilon}$ is the polarization of the incident photon. $g_p$ and $g_n$ are the nucleon magnetic moments. $e^2$ and $f^2$ are respectively the electromagnetic and the meson-nucleon coupling constants. $\delta_1$ and $\delta_3$ are respectively the $T = 1/2$ and $T = 3/2$ S wave phase shifts from pion-nucleon scattering. The quantities $h^{(++)}$ and $h^{(+-)}$ are defined as follows:

$$h^{(++)} = \frac{1}{3}(h_{11} + 4\,h_{13} + 4\,h_{33}) \tag{21}$$

$$h^{(+-)} = \frac{1}{3}(h_{11} + h_{13} - 2\,h_{33}) \tag{22}$$

where, for example,

$$h_{33} = \frac{e^{i\delta_{33}} \sin\delta_{33}}{q^3} \tag{23}$$

and similarly for $h_{11}$ and $h_{13}$. $\delta_{11}$, $\delta_{13}$ and $\delta_{33}$ are the P wave pion-nucleon scattering phase shifts, the first index being twice the isotopic spin of the state in question and the second index twice the angular momentum. The phase shift $\delta_{31}$ does not appear explicitly in the above equations because in this theory it is equal to $\delta_{13}$. Finally $F_S$ is given by

$$F_S = 1 - \tfrac{1}{2}\left(1 + \frac{1-v^2}{2v} \log \frac{1-v}{1+v}\right) \tag{24}$$

where v is the meson C.M. velocity. The first two terms in the amplitude $F^{(+)}$ (equation 20) are P wave terms. The third term is isotropic and is an S wave term. It is a secondary scattering term and interferes with the main P wave term.

As seen from equations 18 and 19, $F^{(0)}$ is proportional to the difference between the amplitudes for negative and positive photomeson production. The most important contribution to $F^{(0)}$ for neutral production is the S wave part that interferes with the P wave terms in $F^{(+)}$. It is given by

$$\frac{1}{ef} F^{(0)} = -i\, \vec{\sigma}\cdot\vec{\varepsilon}\ \ \frac{(g_p+g_n)}{2M}\ w^* \tag{25}$$

where w* is the total energy of the pion plus the final kinetic energy of the nucleon, all in the C.M. system. This "nuclear-recoil term" is a term that did not appear in the older theory.

The cross section may now be calculated from equation 16 and is

$$d\sigma/d\Omega = e^2 f^2 \frac{q}{\nu} \left[ |K_1|^2 + 2q\nu \, \mathrm{Re}\, K_1^* K_2 \cos\theta + q^2\nu^2 \left( |K_2|^2 + |K_3|^2 \right) \frac{\sin^2\theta}{2} + q^2\nu^2 |K_2|^2 \cos^2\theta \right] \tag{26}$$

where

$$K_1 = \frac{g_p + g_n}{2M} w^* + i \frac{2}{3} (\delta_1 - \delta_3) F_S \tag{27}$$

$$K_2 = \frac{g_p - g_n}{4Mf^2} h^{(+-)} \tag{28}$$

and

$$K_3 = \frac{g_p - g_n}{4Mf^2} h^{(++)} \tag{29}$$

It is important to note that this formula for the cross section involves only dipole radiation. The state of the theory is such that the electric quadrupole contribution has not been explicitly calculated and is omitted from consideration here.

Before the cross section is calculated from equation 26 information must be available concerning the scattering phase shifts. $\delta_{33}$ is the most important of the P wave phase shifts. Ashkin et al. (28) give a summary of the experimental values of this phase shift for pion laboratory kinetic energies between 65 and 220 Mev. From

an examination of low energy data Orear (29) finds that $\delta_{33}$ rises as the cube of the pion momentum and is well represented by the formula $\delta_{33} = 13.5\ q^3$ (in degrees) at energies below about 65 Mev. At high energies Margulies (30) has obtained values of $\delta_{33}$ at 260 and 300 Mev. In Russia, Grigoriev and Mitin (31) have measured $\delta_{33}$ at 310 Mev. All of these results are plotted in Fig. 12. Note that the 300 Mev point of Margulies (30) and the Russian (31) point at 310 Mev are quite consistent with each other. The values of $\delta_{33}$ used in the present analysis are taken from the curve of Fig. 12.

The other P wave phase shifts are not as accurately known as $\delta_{33}$. Experimentally the best-fit values of these phase shifts are small with large errors. Also it is difficult to find a trend for any of them in either magnitude or sign. Therefore, for the purposes of the present analysis they are assumed to be zero.

The existing experimental data in regard to the S wave phase shifts, $\delta_1$ and $\delta_3$, does not show the smooth variation with energy as is the case for the phase shift $\delta_{33}$, the various experimental points being somewhat scattered. The data available at the time of the summary of Bethe and de Hoffman (see Fig. 33.1 of reference (11)) seemed to indicate that $\delta_1$ started out positive at low energies, reached a maximum of about $10^\circ$ at a pion energy of 100 Mev and then became negative at about 200 Mev. The behavior of $\delta_3$ was not so complicated; it started out negative and remained negative but did not seem to vary linearly with the pion momentum throughout the energy range up to about 200 Mev. Wigner (32) has shown that there is a lower limit on the derivative of the scattering phase

shift with respect to energy due to the causality condition that a scattered wave cannot reach an observer before the original wave. Orear (33) pointed out that this condition excluded the energy dependence of $\delta_1$ assigned by Bethe and de Hoffmann, and proposed that all pion-nucleon scattering data up to 300 Mev could be fit within limits of experimental error by using the S wave phase shifts linearly extrapolated from the low energy slopes of

$$\delta_1 = 9.2\ q \tag{30}$$

$$\delta_3 = -6.3\ q \tag{31}$$

(in degrees). The results of later experiments (28, 30, 34) agree fairly well with the extrapolations of Orear. Russian experiments (35), however, seem to indicate that the linear extrapolation of $\delta_3$ in equation 31 may be too small in magnitude at pion laboratory kinetic energies above 240 Mev. In the present analysis the S wave phase shifts given by equations 30 and 31 are used throughout the range of pion laboratory kinetic energies from zero to 310 Mev. This assumption seems a reasonable one considering the present experimental data.

Using only $\delta_{33}$, $\delta_1$ and $\delta_3$, the neutral pion photoproduction cross section given in equation 26 can be written

$$d\sigma/d\Omega = A_{33} + A_S + B\cos\theta + C_{33}\cos^2\theta \tag{32}$$

where $A_{33}$ and $A_S$ are the individual contributions to the A coefficient of the magnetic dipole $T = 3/2$, $J = 3/2$ state and S state respectively. The only contribution to the C coefficient comes from

the (3/2, 3/2) state and this is written as $C_{33}$. Explicitly these coefficients are

$$A_{33} = \frac{5}{72}\left(\frac{e}{f}\right)^2 \frac{(g_p-g_n)^2}{M^2} \frac{\nu}{q^3} \sin^2\delta_{33} \tag{33}$$

$$A_S = (ef)^2 \frac{q}{\nu}\left\{\left[\frac{2}{3}(\delta_1-\delta_3)F_S\right]^2 + \left[\frac{1}{2}\frac{(g_p+g_n)}{M} w^*\right]^2\right\} \tag{34}$$

$$B = \frac{1}{3} e^2 \frac{(g_p-g_n)}{M} \frac{\sin\delta_{33}}{q}\left[\frac{2}{3}(\delta_1-\delta_3)F_S\sin\delta_{33} - \frac{1}{2}\frac{(g_p+g_n)}{M} w^* \cos\delta_{33}\right] \tag{35}$$

$$C_{33} = -\frac{3}{5} A_{33} \tag{36}$$

In these equations $\hbar = c = 1$, energies are measured in units of $\mu c^2$ and momenta in units of $\mu c$, $\mu$ is the $\pi^o$ rest energy, $g_p = 2.79$ and $g_n = -1.91$ are in nuclear magnetons. When calculating these coefficients the comparison between scattering and photoproduction is made at the same value of the total energy in the C.M. system. The scattering phase shifts are measured only for the scattering of charged mesons. If $T_{\pi^+}$ is the laboratory kinetic energy of the incident $\pi^+$ meson, then the laboratory energy of the corresponding photon is

$$k = T_{\pi^+} + 150 \text{ Mev} \tag{37}$$

The kinematic quantities $\nu$, q and w* in equations 33 through 36 are calculated assuming the photoproduction of a neutral pion,

whereas the phase shifts are from charged meson scattering data. This discrepancy may lead to serious error at pion energies not much greater than the $\pi^+ - \pi^o$ mass difference, but should not be important in the energy range of the present experiment.

Values of $A_{33}$, $A_S$, B, $C_{33}$, $A = A_{33} + A_S$ and the ratio $-A/C_{33}$ computed from equations 33 through 36 are tabulated in Table V. The coupling constant used is derived from the pion-nucleon scattering data (16) and is $f^2 = 0.08$. The calculated values of A, B and $C_{33}$ are plotted in Fig. 13 as the dashed line. The solid curves for A, B and C are the same as those in Fig. 10. The agreement between the theoretical and experimental A and C coefficients at energies above resonance is very good. The energy at which the experimental and theoretical curves for B cross the zero axis (about 280 Mev) is also in good agreement. As seen from equation 35 this crossover is produced by competition between the secondary scattering and nucleon-recoil S wave terms. The magnitudes of the theoretical values of A and C are somewhat smaller than the experimental values from about 240 Mev to resonance energy. Perhaps inclusion of an electric quadrupole term in the theory would improve the agreement. It is clear, however, that the (3/2, 3/2) magnetic dipole term together with the S wave describes both the magnitude and trend of the neutral pion photoproduction data rather well.

## X. CONCLUSIONS

The new neutral photoproduction data between 260 and 450 Mev indicate that the behavior of the angular distribution coefficients A and C can be explained almost entirely by the magnetic dipole interaction in the (3/2, 3/2) state. The electric quadrupole contribution to the cross section can now be said to be small, a fact that was not evident from previous experimental results. The more accurate experimental information concerning the B coefficient indicates appreciable S wave production above resonance energy.

These results, as well as the crossover-energy of the B coefficient, are consistent with the results of pion-nucleon scattering as shown by the theory of Chew and Low. It is interesting that agreement of the photoproduction and scattering results has been obtained without the use of any adjustable parameters, the only experimental parameters entering being the phase shifts and coupling constant measured in the scattering experiments.

## REFERENCES


1. Walker, Oakley and Tollestrup, Phys. Rev. (1955) 97, 1279-1282. Phys. Rev. (1953) 89, 1301-1302L.
2. D. C. Oakley and R. L. Walker, Phys. Rev. (1955) 97, 1283-1291.
3. Cartwright, Richman, Whitehead and Wilcox, Phys. Rev. (1953) 91, 677-688.
4. Steinberger, Panofsky and Steller, Phys. Rev. (1950) 78, 802-805.
5. Panofsky, Steinberger and Steller, Phys. Rev. (1952) 86, 180-189.
6. C. N. Yang, Phys. Rev. (1950) 77, 242-245.
7. Panofsky, Aamodt and Hadley, Phys. Rev. (1951) 81, 565-574.
8. Brueckner, Serber and Watson, Phys. Rev. (1951) 81, 575-578.
9. B. T. Feld, Phys. Rev. (1953) 89, 330-331L.
10. M. Gell-Mann and K. M. Watson, Annual Rev. of Nuc. Sc. (1954) 4, 219-270.
11. H. Bethe and F. de Hoffmann, Mesons and Fields (1955) Vol. II, Row, Peterson and Co.
12. K. A. Brueckner and K. M. Case, Phys. Rev. (1951) 83, 1141-1147.
13. Watson, Keck, Tollestrup and Walker, Phys. Rev. (1956) 101, 1159-1172.
14. Goldschmidt-Clermont, Osborne and Scott, Phys. Rev. (1953) 89, 329-330L. Phys. Rev. (1955) 97, 188-193.
15. A. Silverman and M. Stearns, Phys. Rev. (1952) 88, 1225-1230.
16. G. F. Chew and F. E. Low, Phys. Rev. (1956) 101, 1570-1579.
17. G. F. Chew and F. E. Low, Phys. Rev. (1956) 101, 1579-1587.

18. Chew, Low, Nambu and Goldberger. To be published. The author wishes to thank Prof. Chew for communicating some of the new results prior to publication.

19. W. K. H. Panofsky and F. L. Fillmore, Phys. Rev. (1950) 79, 57-70.

20. Fay, Gottstein and Hain, Supplemento al Vol. 11, Nuovo Cimento, (1954) No. 2, 234-263.

21. Aron, Hoffman and Williams, AECU-663.

22. T. Yamagata, Ph. D. Thesis, University of Illinois, Nov. 20, 1956.

23. C. Levinthal and A. Silverman, Phys. Rev. (1951) 82, 822-826.

24. J. C. Keck, Phys. Rev. (1952) 85, 410-416.

25. V. Z. Peterson and C. E. Roos, Phys. Rev. In Press.

26. Walker, Teasdale, Peterson and Vette, Phys. Rev. (1955) 99, 210-219.

27. L. J. Koester and F. E. Mills, To be published.

28. Ashkin, Blaser, Feiner and Stern, Phys. Rev. (1957) 105, 724-728.

29. J. Orear, Phys. Rev. (1954) 96, 176-179.

30. R. S. Margulies, Phys. Rev. (1955) 100, 1255 (A).

31. E. L. Grigoriev and N. A. Mitin, Soviet Physics JETP (1957) 4, 10-12.

32. E. P. Wigner, Phys. Rev. (1955) 98, 145-147.

33. J. Orear, Phys. Rev. (1955) 100, 288-291.

34. Ashkin, Blaser, Feiner and Stern, Phys. Rev. (1956) 101, 1149-1158.

35. Mukhin et al., Proceedings of the CERN Symposium at Geneva (1956) 204-224.

TABLE I

Forward angular distribution in C.M. system, $d\sigma/d\Omega$, in units of $10^{-30}$ $cm^2$/ster. "Bare emulsion" data only.

| Photon Energy (Mev) | Pion Angle | | $d\sigma/d\Omega$ |
|---|---|---|---|
| | cos θ | Mean θ | |
| 260 (240-280) | 0.8-0.7 | 41.3° | 9.5 ± 1.0 |
| 260 (240-280) | 0.7-0.5 | 52.8° | 9.9 ± 0.8 |
| 300 (280-320)* | 0.9-0.8 | 31.4° | 10.7 ± 1.2 |
| 300 (280-320)* | 0.8-0.7 | 41.3° | 16.1 ± 1.4 |
| 320 (300-340)* | 0.9-0.8 | 31.4° | 17.2 ± 1.6 |
| 320 (300-340)* | 0.8-0.6 | 45.0° | 21.3 ± 1.4 |
| 360 (340-380) | 0.9-0.8 | 31.4° | 14.8 ± 1.5 |
| 360 (340-380) | 0.8-0.7 | 41.3° | 15.6 ± 1.6 |
| 400 (380-420) | 0.9-0.8 | 31.4° | 10.2 ± 1.2 |
| 450 (420-480) | 0.9-0.8 | 31.4° | 6.7 ± 1.0 |

*Overlapping data regrouped to allow direct comparison with Oakley and Walker (2) data.

TABLE II

| Plate | Area Scanned ($cm^2$) | Scanning Efficiency (%) | Number of Events | Laboratory Scanned |
|---|---|---|---|---|
| 1 | 0.90 | $95 \pm 2$ | 144 | Cal Tech |
| 2 | 2.74 | $95 \pm 2$ | 388 | Cal Tech |
| 3 | 5.71 | $95 \pm 2$ | 756 | Cornell |
| 4 | 2.26 | $75 \pm 3$ | 237 | Cornell |

TABLE III

"Under-carbon" differential cross-sections compared to Oakley and Walker (2) values.

$d\sigma/d\Omega$ in units of $10^{-30}$ $cm^2$/ster.

| Mean k | Mean $\theta$ | No. of events | $d\sigma/d\Omega$ | Oakley and Walker $d\sigma/d\Omega$ | Ratio |
|---|---|---|---|---|---|
| 300 Mev | $87^o$ | 83 | 23.2 | 23.5 | $.99 \pm .13$ |
| 320 Mev | $80^o$ | 63 | 20.0 | 25.0 | $.80 \pm .15$ |
| 360 Mev | $60^o$ | 60 | 23.4 | 18.0 | $1.30 \pm .18$ |
| | | | | Average = | $1.02 \pm .09$ |

TABLE IV

A, B and C coefficients in units of $10^{-30}$ $cm^2$/ster.

| k | 260 | 300 | 320 | 360 | 400 | 450 |
|---|---|---|---|---|---|---|
| A | 13.9±0.7 | 23.8±0.7 | 26.6±0.6 | 20.9±0.7 | 14.1±0.4 | 8.0±0.5 |
| B | 0.2±0.6 | -0.4±0.7 | 2.7±0.8 | 2.8±0.7 | 3.0±0.7 | 2.4±0.6 |
| C | -9.2±1.7 | -15.9±1.4 | -15.6±1.3 | -12.8±1.4 | -9.1±1.1 | -4.7±0.8 |
| -A/C | 1.52±0.29 | 1.50±0.14 | 1.70±0.15 | 1.64±0.19 | 1.55±0.19 | 1.69±0.28 |

Average value of A/C = -1.60 ± 0.10

TABLE V

Values of $A_{33}$, $A_S$, B, $C_{33}$, $A = A_{33} + A_S$ and the ratio $-A/C_{33}$ calculated from equations 33 through 36 in units of $10^{-30}$ $cm^2$/ster.

| k | $A_{33}$ | $A_S$ | B | $C_{33}$ | A | $-A/C_{33}$ |
|---|---|---|---|---|---|---|
| 160 | .064 | .041 | -.050 | -.038 | .105 | 2.74 |
| 180 | .563 | .106 | -.185 | -.338 | .669 | 1.98 |
| 200 | 1.46 | .177 | -.322 | -.876 | 1.64 | 1.86 |
| 220 | 2.79 | .245 | -.431 | -1.67 | 3.04 | 1.82 |
| 240 | 5.40 | .316 | -.480 | -3.24 | 5.72 | 1.77 |
| 260 | 8.74 | .392 | -.354 | -5.24 | 9.13 | 1.74 |
| 280 | 13.7 | .458 | .139 | -8.22 | 14.2 | 1.73 |
| 300 | 19.2 | .529 | 1.13 | -11.5 | 19.7 | 1.71 |
| 320 | 23.3 | .595 | 2.49 | -14.0 | 23.9 | 1.71 |
| 340 | 24.1 | .665 | 3.99 | -14.5 | 24.8 | 1.71 |
| 360 | 20.2 | .738 | 4.54 | -12.1 | 20.9 | 1.73 |
| 380 | 16.0 | .814 | 4.47 | -9.60 | 16.8 | 1.75 |
| 400 | 13.1 | .880 | 4.26 | -7.86 | 14.0 | 1.78 |
| 420 | 10.6 | .957 | 4.03 | -6.36 | 11.6 | 1.82 |
| 440 | 9.02 | 1.03 | 3.86 | -5.41 | 10.0 | 1.86 |
| 460 | 7.64 | 1.10 | 3.67 | -4.58 | 8.74 | 1.91 |

## FIGURE CAPTIONS

Fig. 1. Schematic of the experimental arrangement of emulsion pellicles in the hydrogen gas target.

Fig. 2. Schematic of the emulsion geometry looking directly into the beam.

Fig. 3. Typical range vs. angle plot of protons ending in a 600 micron pellicle. The solid lines denote constant photon energy and pion C. M. angle. The dashed lines are limiting ranges (see text). This plot represents 58 per cent of the total "bare emulsion" data.

Fig. 4. Schematic showing the "under carbon" geometry.

Fig. 5. Plot of the "under carbon" detection efficiency.

Fig. 6. Histogram showing the angular distribution of background protons of energy less than 20 Mev at angles between $80^{\circ}$ and the geometrical cutoff angle of $105^{\circ}$.

Fig. 7. Angular distributions for k = 260 Mev and 300 Mev. The open circles are the present results and the solid circles are the results of Oakley and Walker. The crosses are the 260 Mev results of Goldschmidt-Clermont, Osborne and Scott. The solid curves are least squares fits to the combined Oakley and Walker and present data assuming $d\sigma/d\Omega = A + B \cos\theta + C \cos^2\theta$. Two uncertainties are shown for the present experimental points, the "inside" uncertainties representing standard deviations due to statistics only, and the "outside" uncertainties are the total standard deviations.

Fig. 8. Angular distributions for k = 320 Mev and 400 Mev. The solid lines are least squares fits to the combined Oakley and Walker data and the present data. The dashed lines are least squares fits to the Oakley and Walker data only.

Fig. 9. Angular distributions for k = 360 Mev and 450 Mev. The solid curves are least squares fits to the combined Oakley and Walker data and the present data. The dashed lines are least squares fits to the Oakley and Walker data only.

Fig. 10. Coefficients of the angular distribution $d\sigma/d\Omega = A + B \cos\theta + C \cos^2\theta$ plotted as a function of photon energy. The dashed curves for A and C are the experimental values of A and C adopted by Watson et al. (13). The dashed curve for B is that given by Oakley and Walker, and is a fit to their data for B and the MIT B data (14). The solid curves for A, B and C are visual fits to the present results and the Illinois data (27).

Fig. 11. Total cross sections as calculated from the A and C coefficients given by the curves in Fig. 8, except that below 245 Mev the solid curve is that given by Koester and Mills (27) from their measurements of the total cross section.

Fig. 12. Values of the scattering phase shift $\delta_{33}$.

Fig. 13. Comparison of the experimental angular distribution coefficients with those calculated from the theory of Chew and Low. The solid curve is taken from Fig. 10.

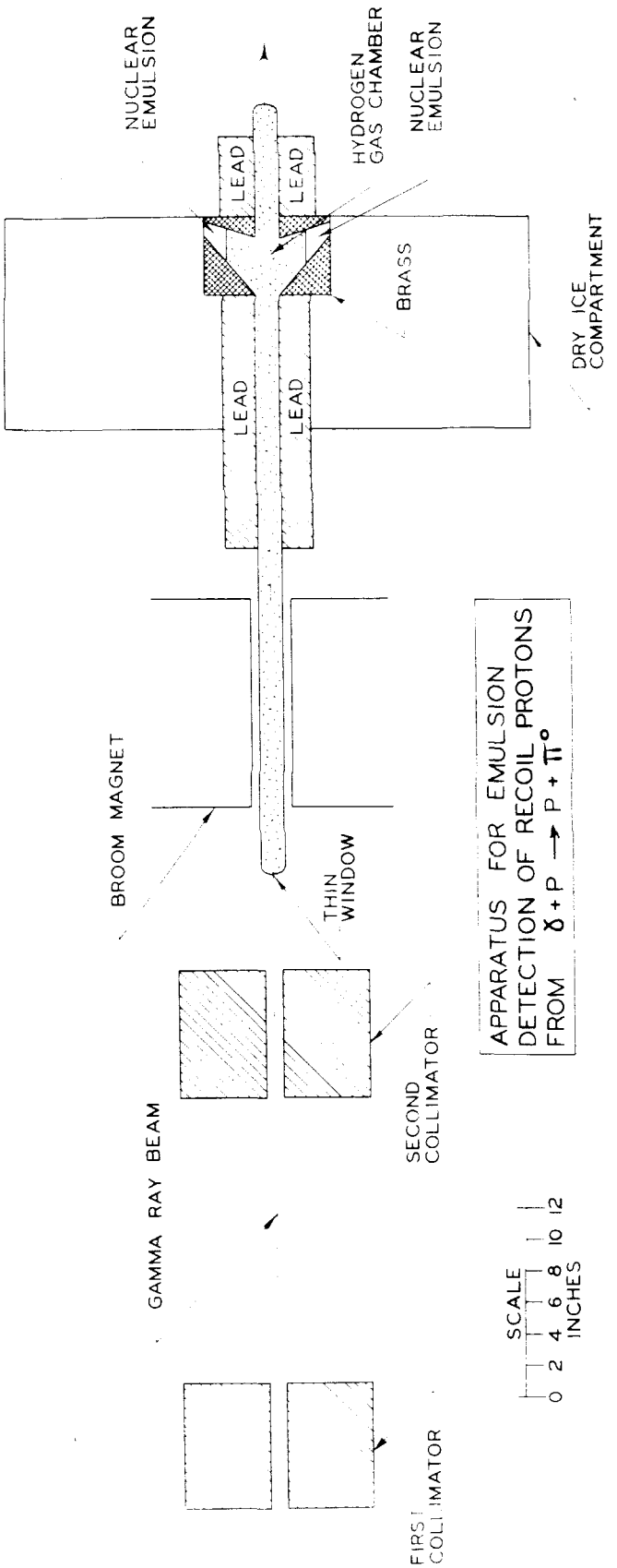
NUCLEAR EMULSION
LEAD
LEAD
HYDROGEN GAS CHAMBER
NUCLEAR EMULSION
BRASS
DRY ICE COMPARTMENT
LEAD
LEAD
BROOM MAGNET
THIN WINDOW
SECOND COLLIMATOR
GAMMA RAY BEAM
FIRST COLLIMATOR
APPARATUS FOR EMULSION DETECTION OF RECOIL PROTONS FROM γ + P → P + π°
SCALE
0 2 4 6 8 10 12
INCHES

Fig. 1

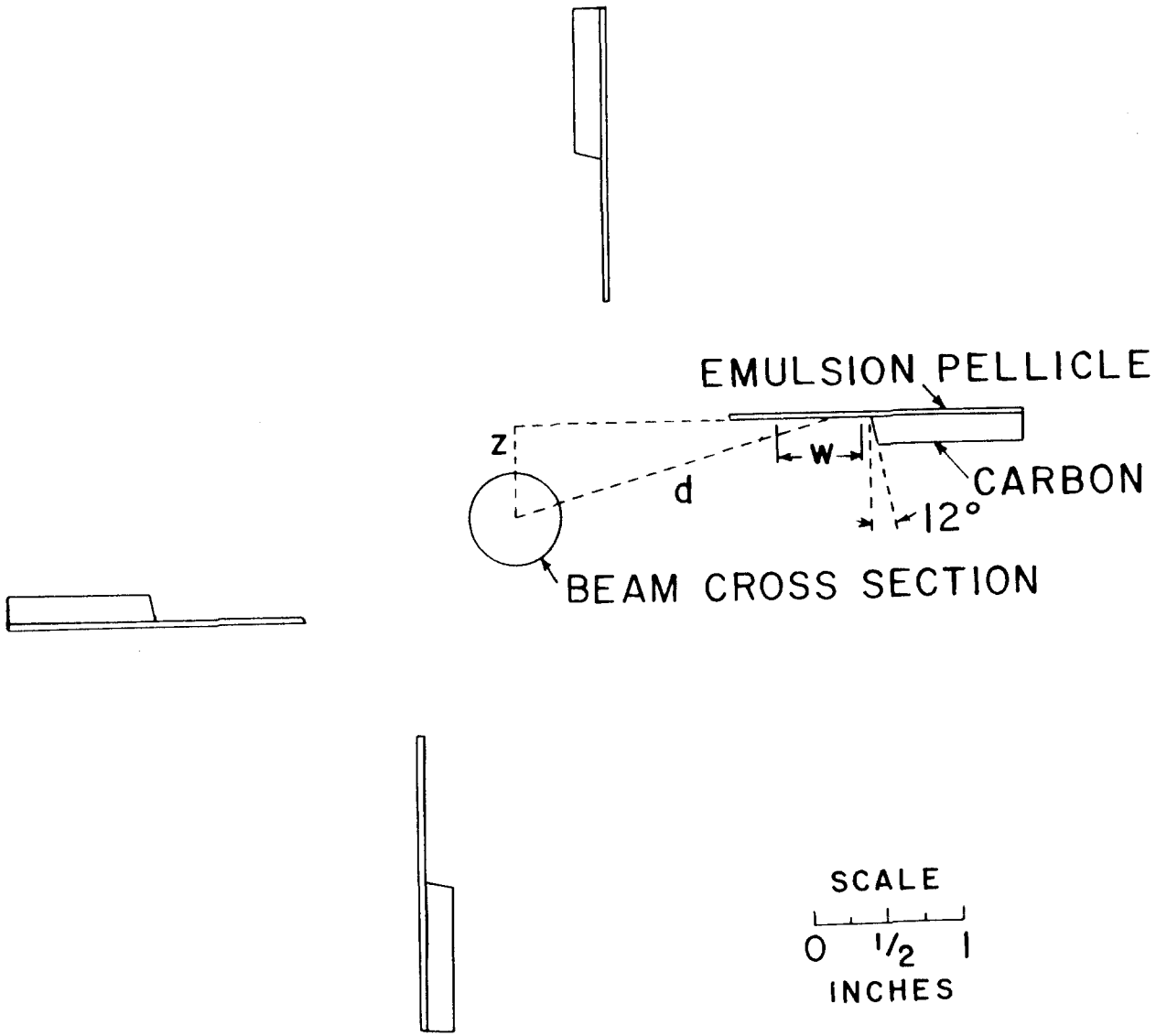
EMULSION PELLICLE
z
w
d
CARBON
12°
BEAM CROSS SECTION
SCALE
0 1/2 1
INCHES

Fig. 2

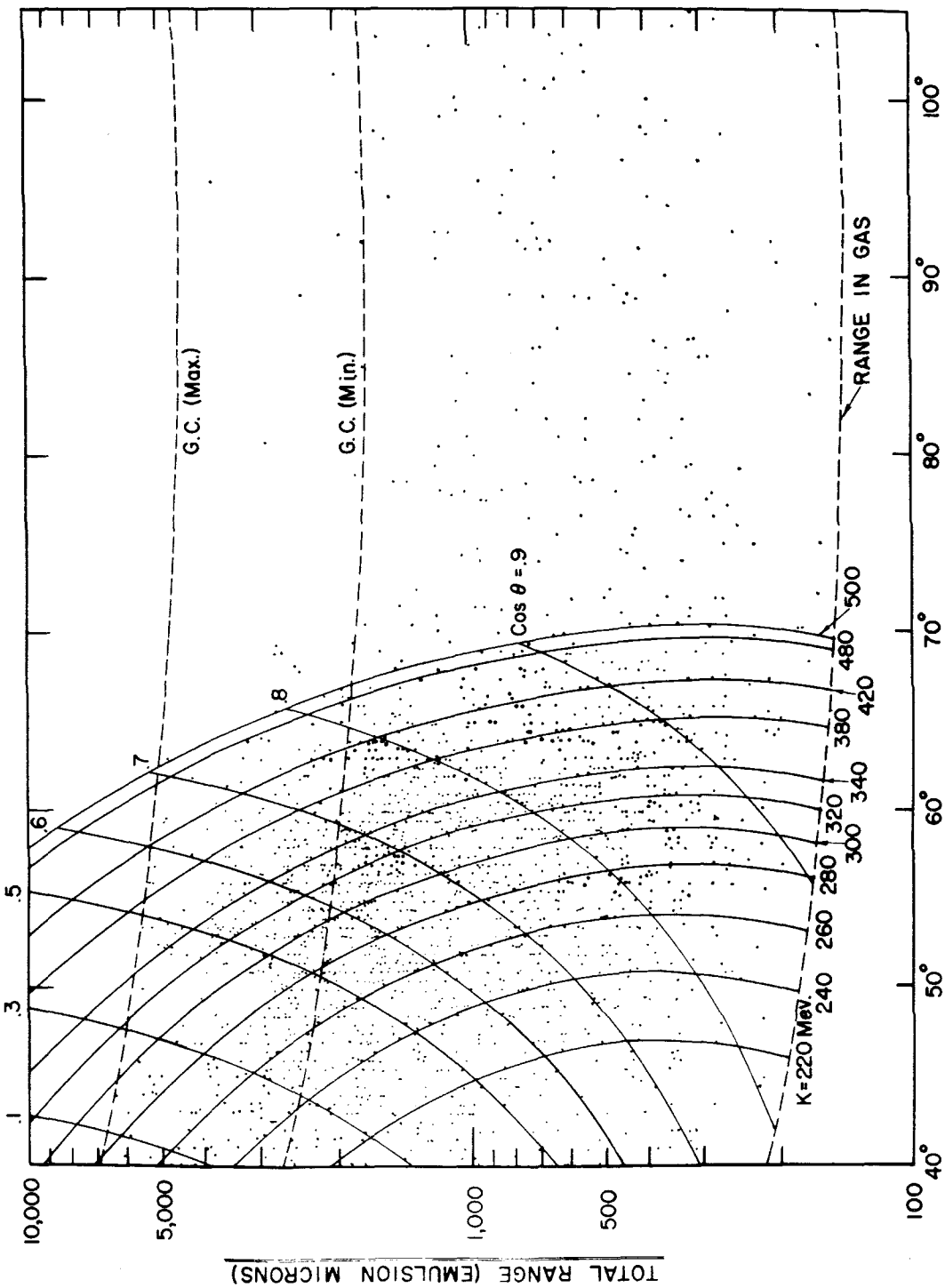
G.C. (Max.)
G.C. (Min.)
RANGE IN GAS
Cos θ = .9
.8
.7
.6
.5
.3
.1
500
480
420
380
340
320
300
280
260
240
K=220 Mev.
10,000
5,000
1,000
500
100
40°
50°
60°
70°
80°
90°
100°
TOTAL RANGE (EMULSION MICRONS)
PROTON LAB ANGLE

Fig. 3

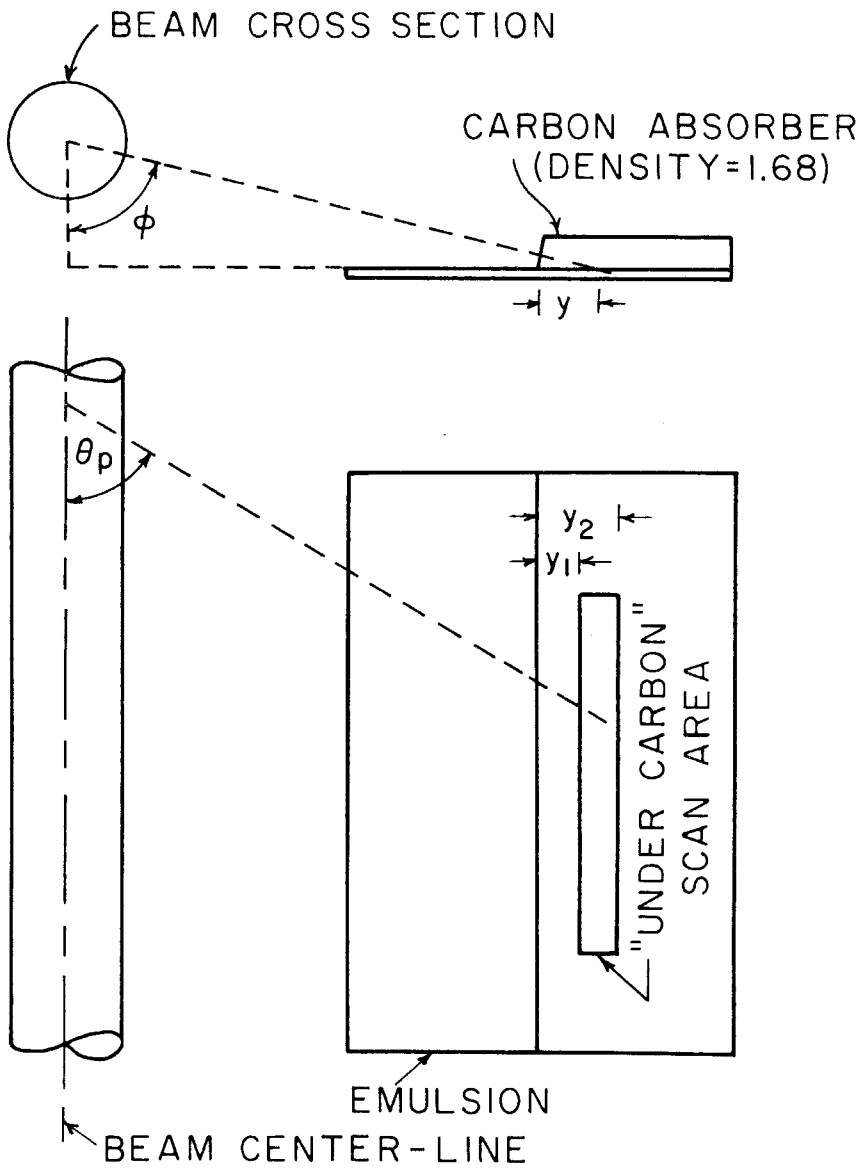


"UNDER CARBON" EMULSION GEOMETRY

Fig. 4

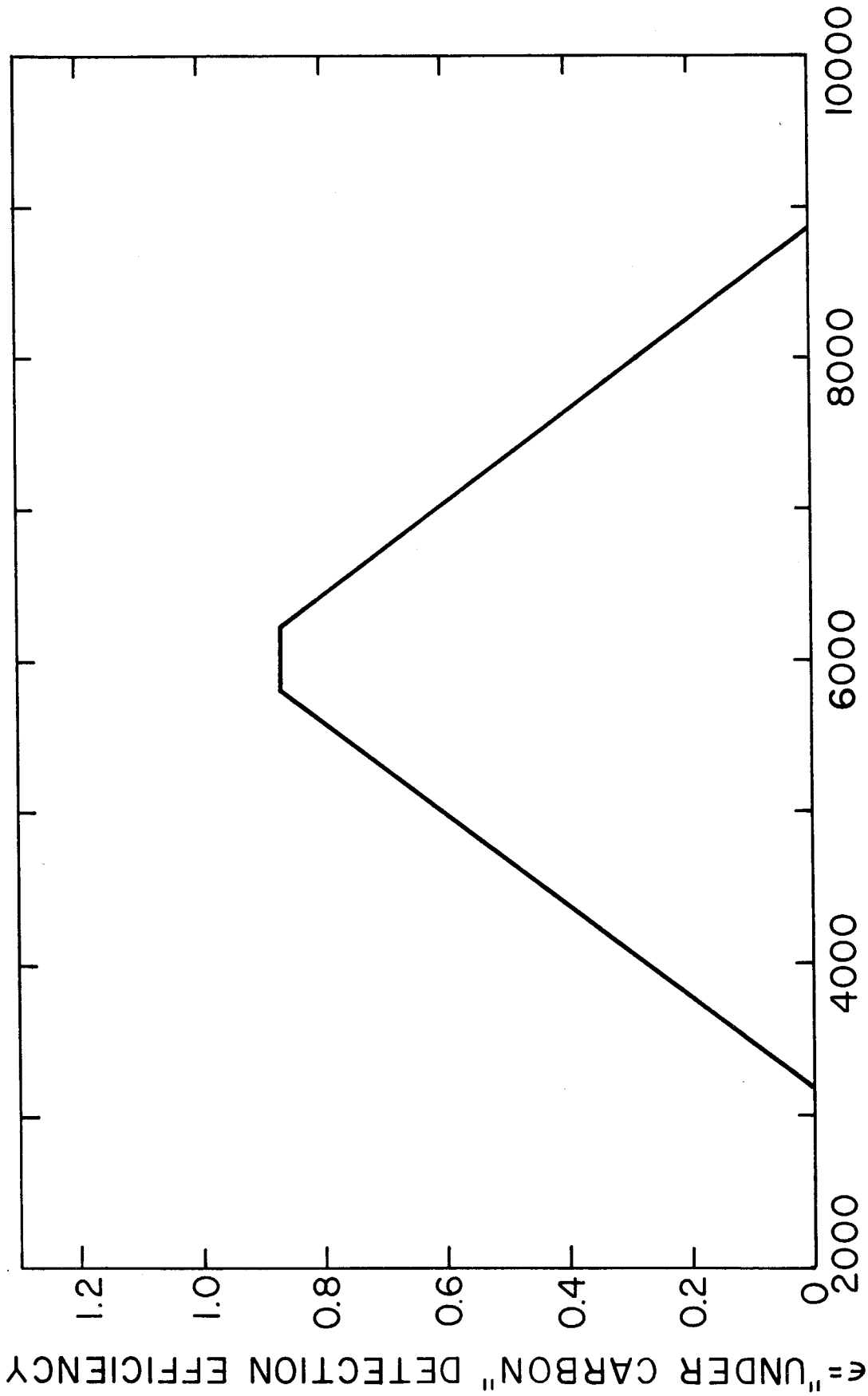
ε="UNDER CARBON" DETECTION EFFICIENCY
0
0.2
0.4
0.6
0.8
1.0
1.2
2000
4000
6000
8000
10000
R SIN θp (MICRONS OF EMULSION EQUIVALENT)

Fig. 5

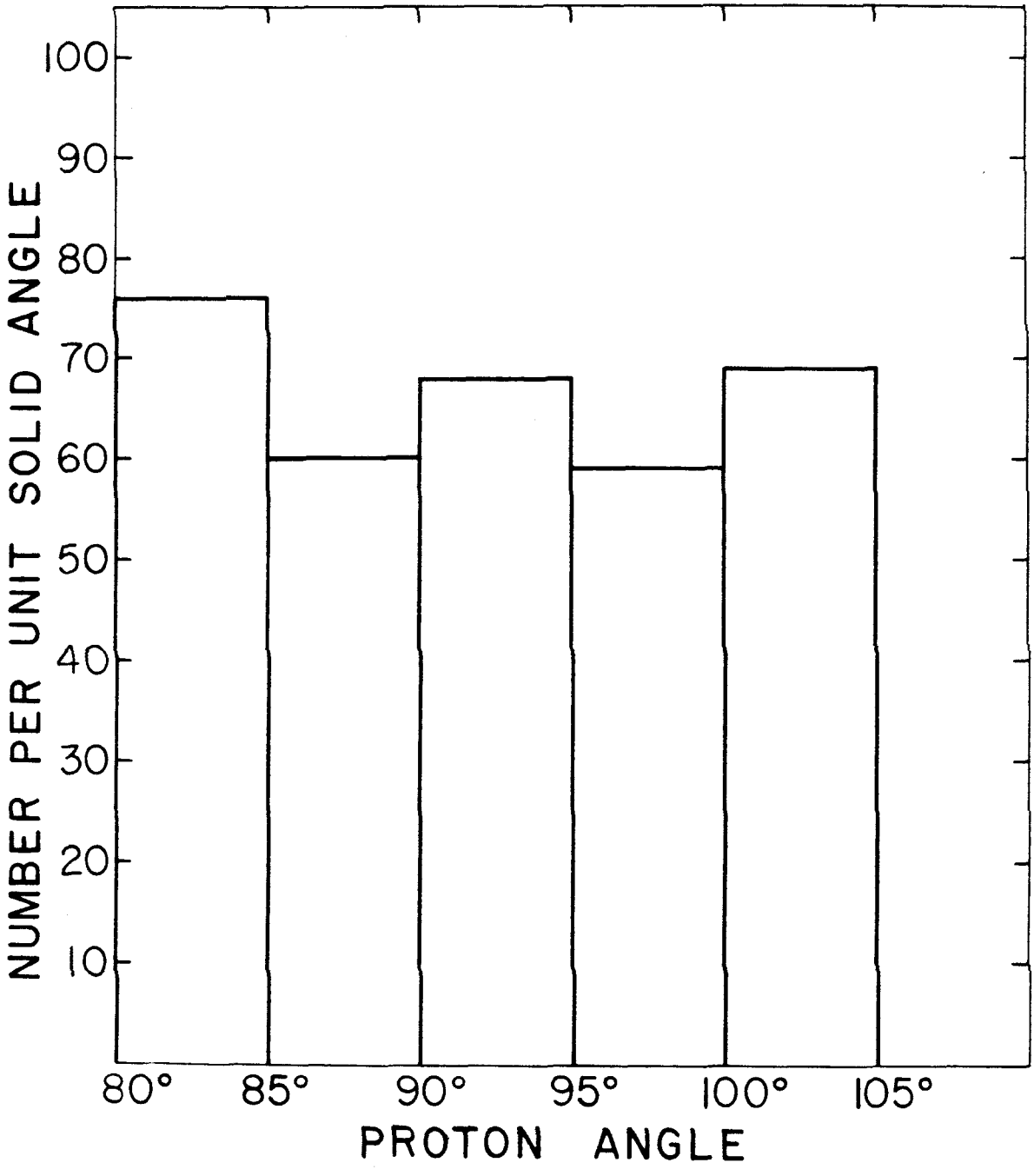
NUMBER PER UNIT SOLID ANGLE
100
90
80
70
60
50
40
30
20
10
80°
85°
90°
95°
100°
105°
PROTON ANGLE

Fig. 6

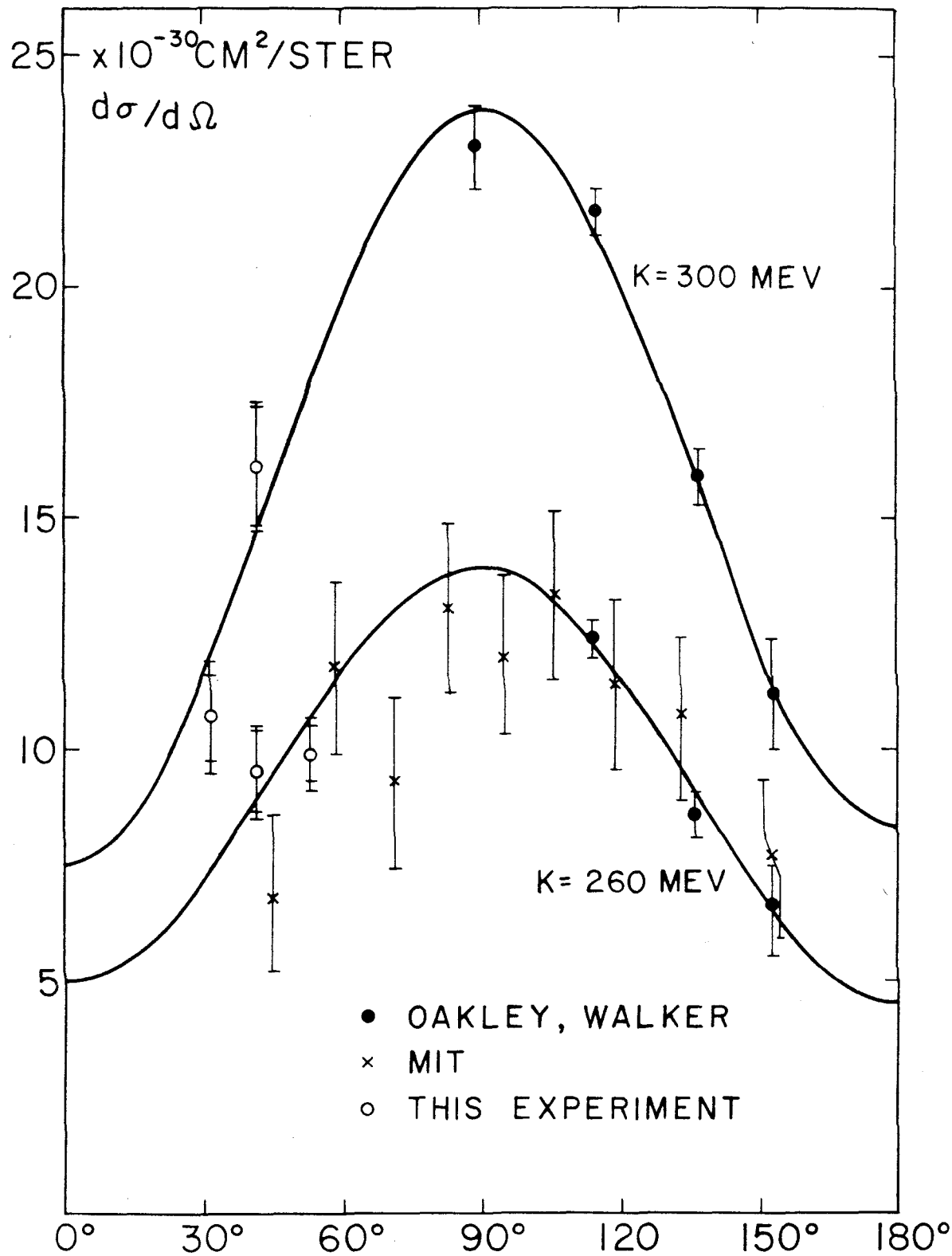
25
20
15
10
5
x10⁻³⁰CM²/STER
dσ/dΩ
K= 300 MEV
K= 260 MEV
● OAKLEY, WALKER
× MIT
○ THIS EXPERIMENT
0°
30°
60°
90°
120
150°
180°
π° C.M. ANGLE

Fig. 7

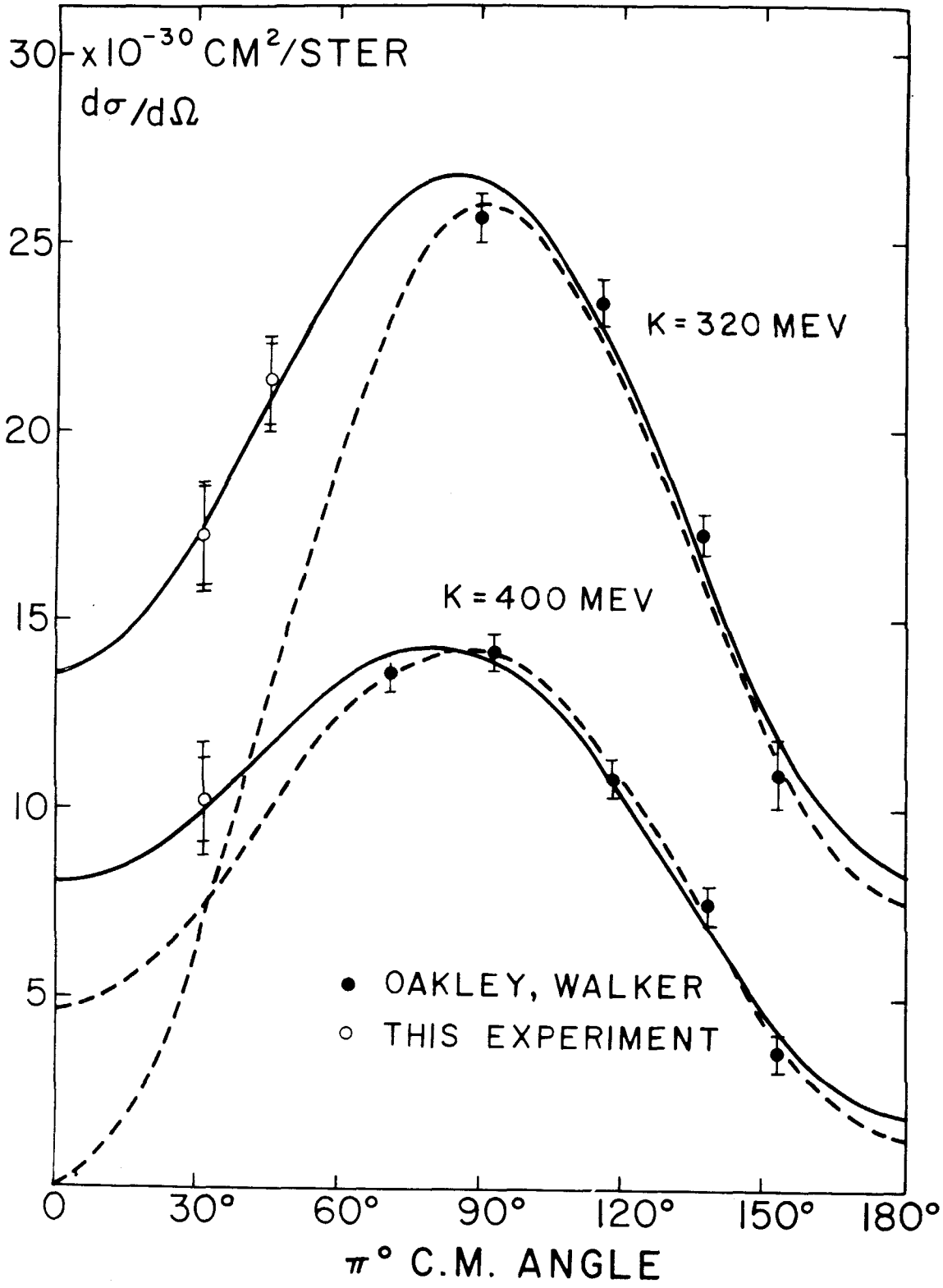
30
25
20
15
10
5
0
30°
60°
90°
120°
150°
180°
x10⁻³⁰ CM²/STER
dσ/dΩ
K = 320 MEV
K = 400 MEV
● OAKLEY, WALKER
○ THIS EXPERIMENT
π° C.M. ANGLE

Fig. 8

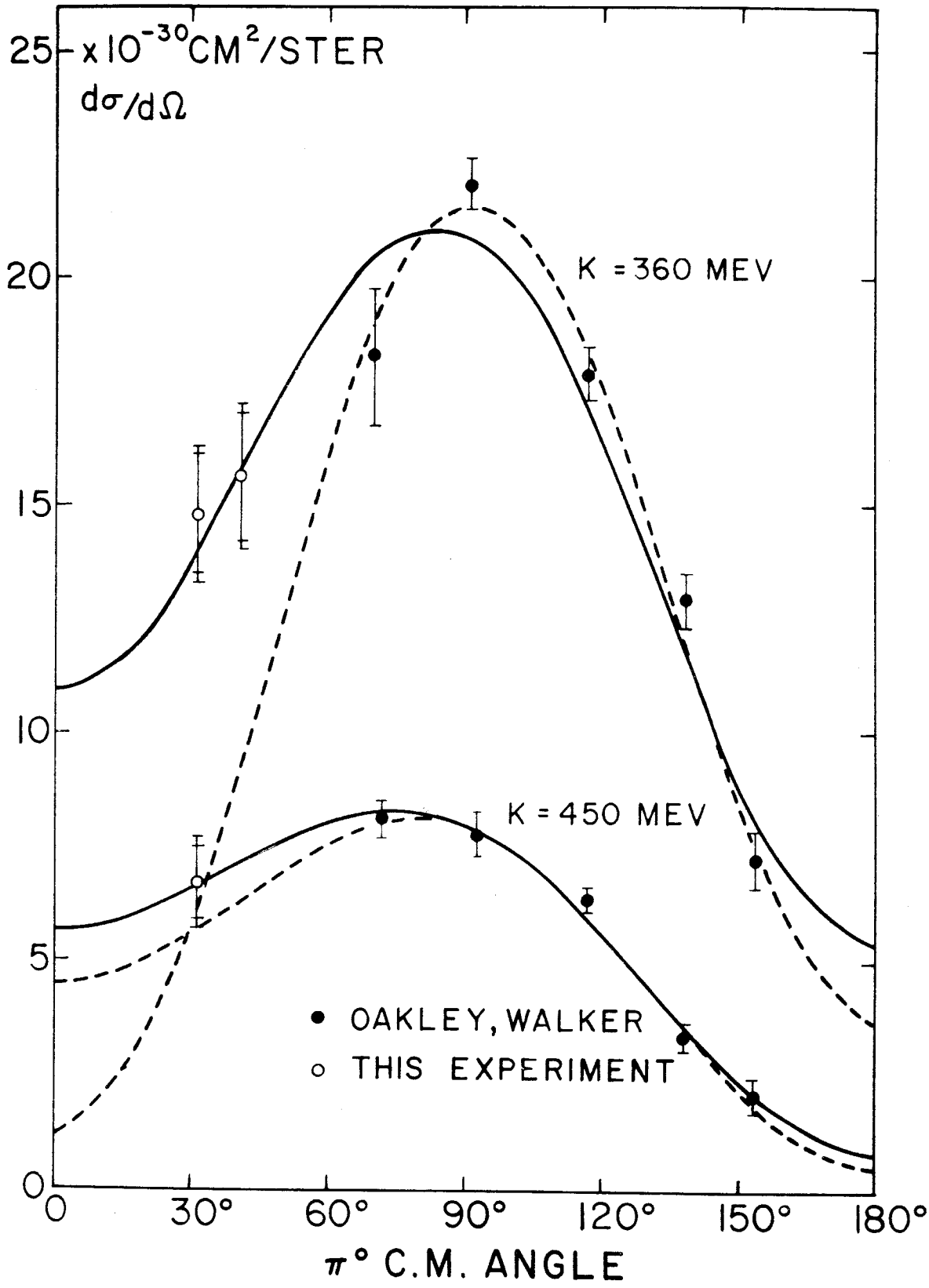
25
x10^-30 CM^2/STER
dσ/dΩ
20
15
10
5
0
K = 360 MEV
K = 450 MEV
OAKLEY, WALKER
THIS EXPERIMENT
0
30°
60°
90°
120°
150°
180°
π° C.M. ANGLE

Fig. 9

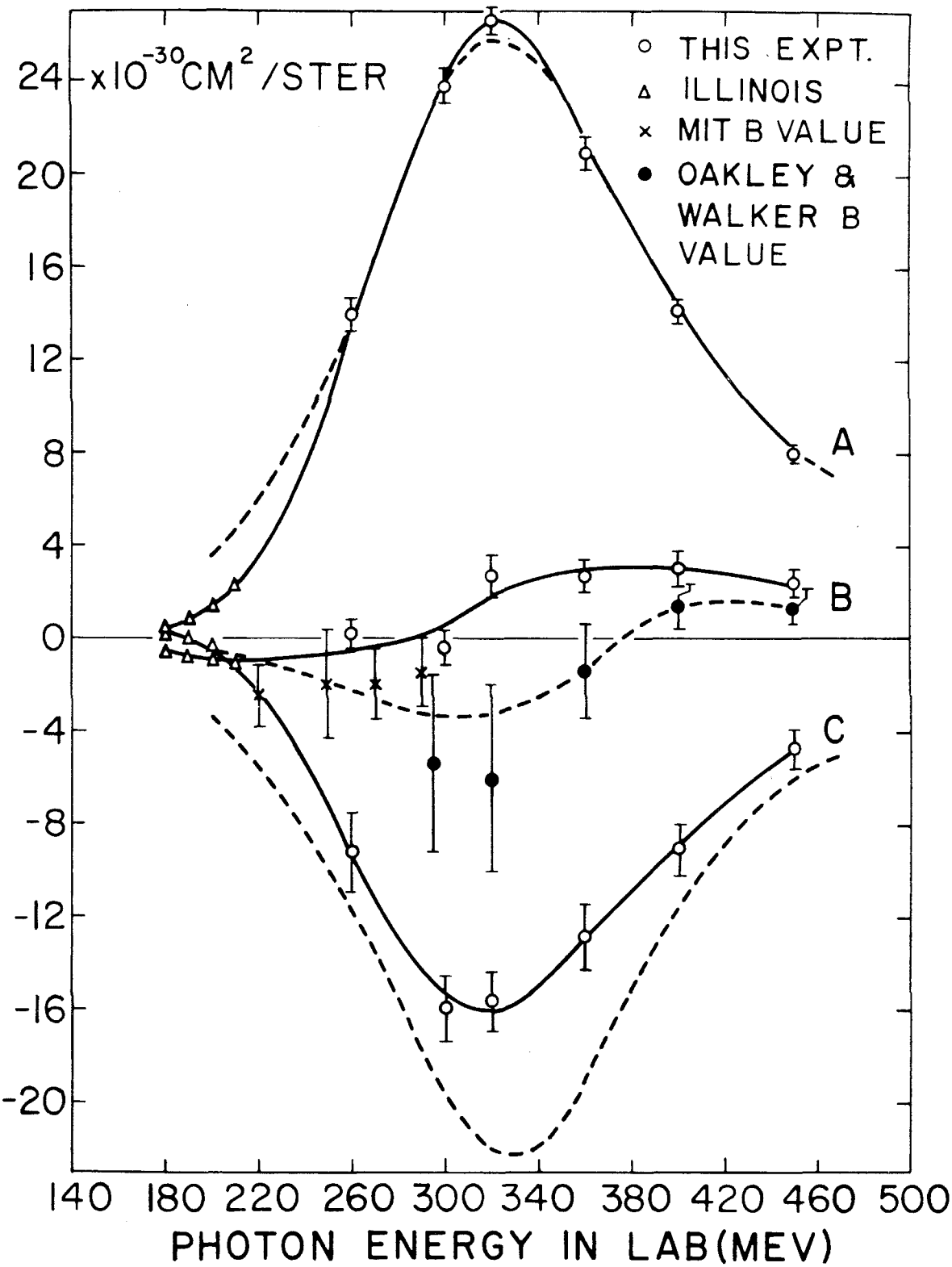
24
20
16
12
8
4
0
-4
-8
-12
-16
-20
x10^-30 CM^2 /STER
THIS EXPT.
ILLINOIS
MIT B VALUE
OAKLEY & WALKER B VALUE
A
B
C
140 180 220 260 300 340 380 420 460 500
PHOTON ENERGY IN LAB(MEV)

Fig. 10

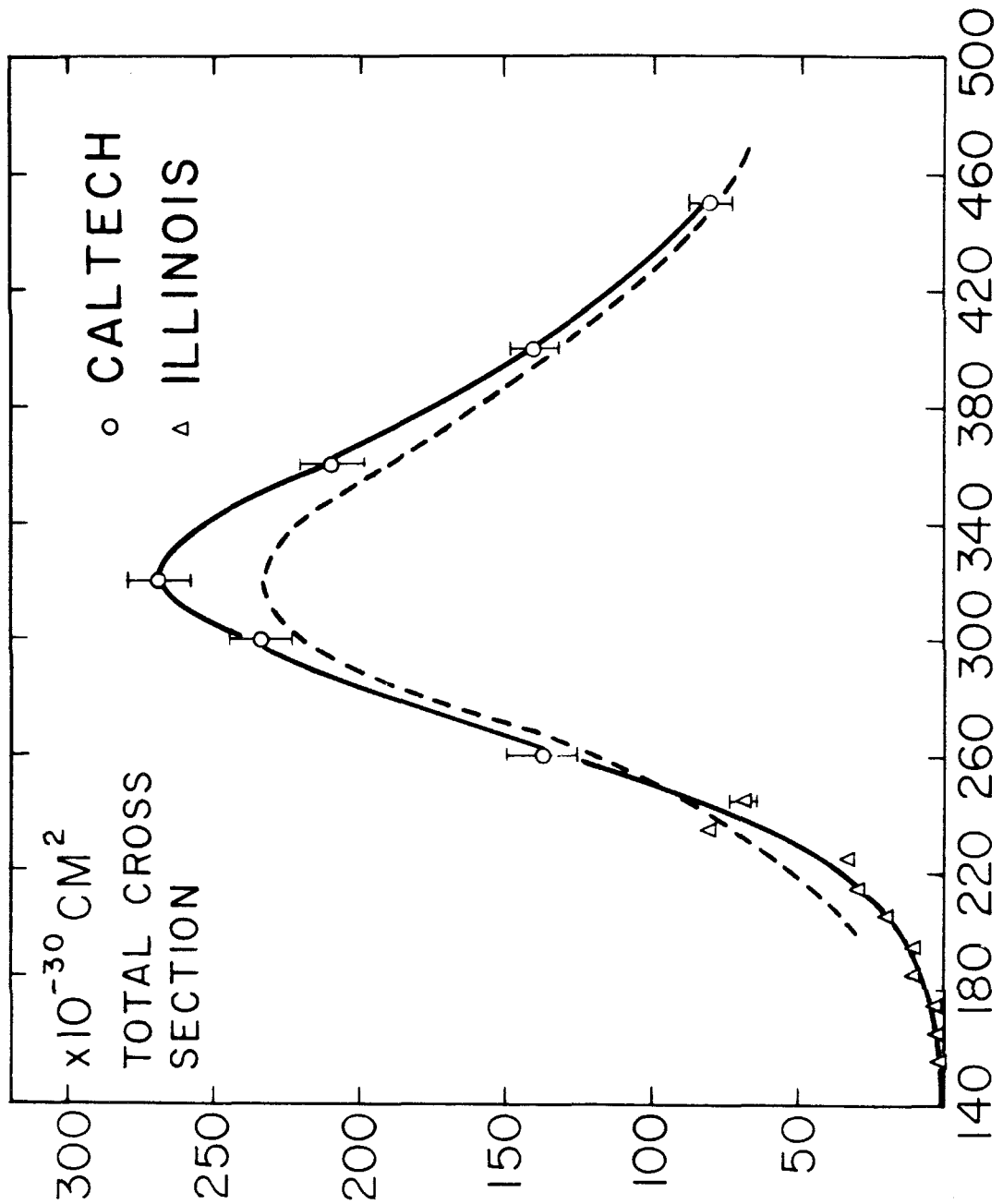
o CALTECH
Δ ILLINOIS
TOTAL CROSS SECTION
x10^-30 CM^2
300
250
200
150
100
50
140 180 220 260 300 340 380 420 460 500
PHOTON ENERGY IN LAB(MEV)

Fig. 11

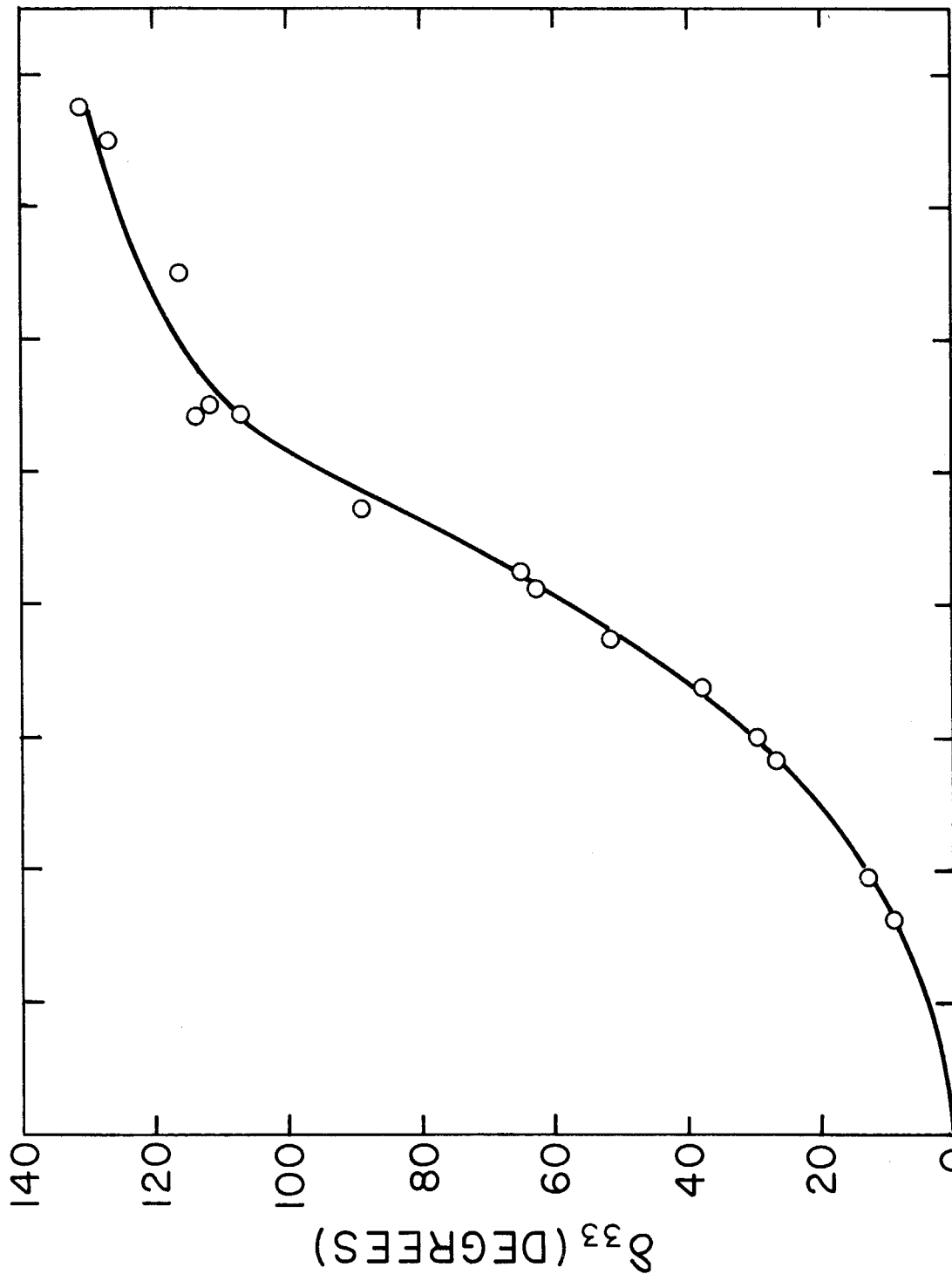


Fig. 12 LABORATORY KINETIC ENERGY OF PION

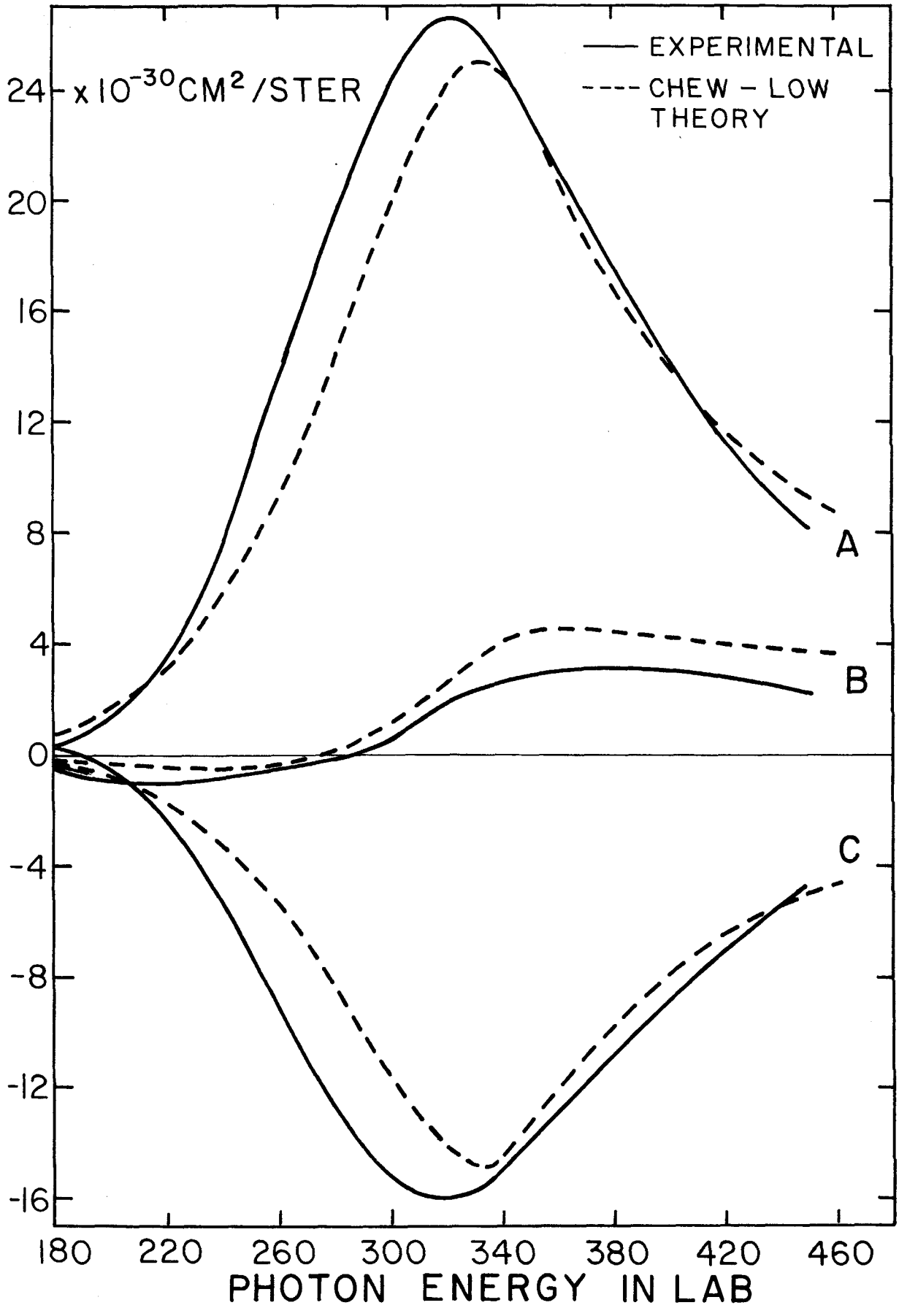
EXPERIMENTAL
CHEW – LOW THEORY
x 10⁻³⁰ CM² /STER
24
20
16
12
8
4
0
-4
-8
-12
-16
A
B
C
180
220
260
300
340
380
420
460
PHOTON ENERGY IN LAB

Fig. 13